

A THEORETICAL INTERPRETATION OF THE BLACK HOLE FUNDAMENTAL PLANE

PHILIP F. HOPKINS¹, LARS HERNQUIST¹, THOMAS J. COX¹, BRANT ROBERTSON², & ELISABETH KRAUSE³

Accepted to ApJ, May 2007

ABSTRACT

We examine the origin and evolution of correlations between properties of supermassive black holes (BHs) and their host galaxies using simulations of major galaxy mergers, including the effects of gas dissipation, cooling, star formation, and BH accretion and feedback. We demonstrate that the simulations predict the existence of a BH “fundamental plane” (BHFP), of the form $M_{\text{BH}} \propto \sigma^{3.0 \pm 0.3} R_e^{0.43 \pm 0.19}$ or $M_{\text{BH}} \propto M_*^{0.54 \pm 0.17} \sigma^{2.2 \pm 0.5}$, similar to relations found observationally. The simulations indicate that the BHFP can be understood roughly as a tilted intrinsic correlation between BH mass and spheroid binding energy, or the condition for feedback coupling to power a pressure-driven outflow. While changes in halo circular velocity, merger orbital parameters, progenitor disk redshifts and gas fractions, ISM gas pressurization, and other parameters can drive changes in e.g. σ at fixed M_* , and therefore changes in the $M_{\text{BH}} - \sigma$ or $M_{\text{BH}} - M_*$ relations, the BHFP is robust. Given the empirical trend of decreasing R_e for a given M_* at high redshift (i.e. increasingly deep potential wells), the BHFP predicts that BHs will be more massive at fixed M_* , in good agreement with recent observations. This evolution in the structural properties of merger remnants, to smaller R_e and larger σ (and therefore larger M_{BH} , conserving the BHFP) at a given M_* , is driven by the fact that disks (merger progenitors) have characteristically larger gas fractions at high redshifts. Adopting the observed evolution of disk gas fractions with redshift, our simulations predict the observed trends in both $R_e(M_*)$ and $M_{\text{BH}}(M_*)$. The existence of this BHFP also has important implications for the masses of the very largest black holes, and immediately resolves several apparent conflicts between the BH masses expected and measured for outliers in both the $M_{\text{BH}} - \sigma$ and $M_{\text{BH}} - M_*$ relations.

Subject headings: quasars: general — galaxies: active — galaxies: evolution — cosmology: theory

1. INTRODUCTION

Correlations between the masses of supermassive black holes (BHs) in the centers of galaxies and the properties of their host spheroids (e.g., Kormendy & Richstone 1995) imply a fundamental bond between the growth of BHs and galaxy formation. A variety of such correlations have been identified, linking BH mass to host luminosity (Kormendy & Richstone 1995), mass (Magorrian et al. 1998), velocity dispersion (Ferrarese & Merritt 2000; Gebhardt et al. 2000), concentration or Sersic index (Graham et al. 2001; Graham & Driver 2006), and binding energy (Aller & Richstone 2007). However, the connection between these relationships is obscured by the fact that the properties of the host spheroids are themselves correlated (see e.g. Novak et al. 2006, for a comparison of the observed relations). The lack of a clear motivation for favoring one correlation over another has led to considerable debate over the interpretation of systems deviating from the mean correlation between host properties, and over the demographics of the most massive BHs (e.g., Bernardi et al. 2006; Lauer et al. 2006b; Batcheldor et al. 2006; Wyithe 2006).

Analytical estimates (e.g., Silk & Rees 1998; Burkert & Silk 2001) and studies using simulations (Cox et al. 2006b; Robertson et al. 2006b) have demonstrated that these correlations, in particular the $M_{\text{BH}} - \sigma$ (Di Matteo et al. 2005) and $M_{\text{BH}} - M_*$ (Robertson et al. 2006c) relations, can be reproduced in feedback-regulated

models of BH growth. However, determining the fundamental character and evolution of these correlations with redshift is critical for informing analytical models (e.g., Croton 2006) and simulations (Di Matteo et al. 2005; Robertson et al. 2006c; Hopkins et al. 2005) which follow the co-formation of BHs and bulges, as well as theories which relate the evolution and statistics of BH formation and quasar activity to galaxy mergers (e.g., Hopkins et al. 2006a, 2007f, 2006e, 2007c) and to the remnant spheroid population (Hopkins et al. 2006c, 2007b). Likewise, the significance of observations tracing the buildup of spheroid populations (e.g., Cowie et al. 1996) and associations between spheroids in formation, mergers, and quasar hosts (Hopkins et al. 2007a) depends on understanding the evolution of BH/host correlations.

Unfortunately, efforts to directly infer these correlations at redshifts $z \gg 0$ are difficult and still limited by the small number of observable hosts. Furthermore, without understanding the fundamental nature of the correlations between BH and host properties, it is difficult to interpret these observations, as they do not all probe the same correlations. Consequently, different groups have arrived at seemingly contradictory conclusions. Velocity dispersion measurements have favored both no evolution (Shields et al. 2003, from OIII velocity dispersions) and substantial evolution (Shields et al. 2006; Woo et al. 2006, from CO dispersions and spectral template fitting). BH clustering measurements (Adelberger & Steidel 2005; Wyithe & Loeb 2005; Hopkins et al. 2007e; Lidz et al. 2006) suggest moderate evolution in the ratio of BH to host halo mass at redshifts $z \sim 1 - 3$. Direct host *R*-band luminosity measurements (Peng et al. 2006) and indirect comparison of quasar luminosity and stellar mass densities (Merloni et al. 2004) or BH and stellar mass functions (Hopkins et al. 2006d) similarly favor moderate evolution in the ratio of BH to

¹ Harvard-Smithsonian Center for Astrophysics, 60 Garden Street, Cambridge, MA 02138

² Kavli Institute for Cosmological Physics, The University of Chicago, 5460 S. Ellis Ave., Chicago, IL 60637

³ Department of Physics and Astronomy, Universität Bonn, 53121 Bonn, Germany

host spheroid stellar mass occurring at $z \gtrsim 1$, and dynamical masses from CO measurements suggest that this evolution may extend to $z \sim 6$ (Walter et al. 2004). Better understanding the dependence of BH mass on host properties can provide both a self-consistent paradigm in which to interpret these observations and (potentially) a physically and observationally motivated prediction of their evolution.

One possibility is that these different correlations are projections of the same “fundamental plane” (FP) relating BH mass with two or more spheroid properties such as stellar mass, velocity dispersion, or effective radius, in analogy to the well-established fundamental plane of spheroids. For the case of spheroids, it is now understood that various correlations, including the Faber-Jackson relation (Faber & Jackson 1976) between luminosity (or effectively stellar mass M_*) and velocity dispersion σ , the Kormendy (1977) relation between effective radius R_e and surface brightness I_e , and the size-luminosity or size-mass relations (e.g., Shen et al. 2003) between R_e and M_* , are all projections of a fundamental plane relating $R_e \propto \sigma^\alpha I_e^\beta$ (Dressler et al. 1987; Djorgovski & Davis 1987).

In their analysis of the relation between BH mass and host luminosity or dynamical mass, M_{dyn} , Marconi & Hunt (2003) (see also de Francesco et al. 2006) noted that the residuals of the $M_{\text{BH}} - \sigma$ relation (effectively M_{BH}/σ^4 ; Tremaine et al. 2002) were significantly correlated with the effective radii of the systems in their sample. A more detailed study by Hopkins et al. (2007d) (henceforth Paper I) found that the observations indeed favor a fundamental plane-type relation between M_{BH} and any two of R_e , σ , or M_* , at $> 3\sigma$ confidence. This observed, low redshift BHFP has the form $M_{\text{BH}} \propto \sigma^{3.0 \pm 0.3} R_e^{0.43 \pm 0.19}$ or $M_{\text{BH}} \propto M_*^{0.54 \pm 0.17} \sigma^{2.2 \pm 0.5}$, with the early-type FP providing a tight mapping between M_* , R_e , and σ . Given the mean correlations between e.g. R_e and M_* or M_* and σ , the previously recognized correlations between BH mass and spheroid mass, luminosity, velocity dispersion, and binding energy can all naturally be explained as projections of this intrinsic BHFP. However, these observations remain limited in the range of systems they probe, and are restricted to passive, local spheroids. We therefore wish both to understand the origin of this BHFP and how it should (or should not) evolve with redshift.

In this paper, we investigate the nature of the correlation between BH mass and host properties and the existence of a fundamental plane relating BH mass and spheroid mass, velocity dispersion, and effective radius. In § 3, we describe a large set of numerical simulations which we use to study and predict the nature of the BH-host correlations under a wide variety of conditions, and in § 2 we describe the observational data sets we compile to study the observed correlations. In § 4 we describe the correlations determined from both simulations and observations, and then analyze the correlations between residuals in e.g. the $M_{\text{BH}} - \sigma$ relation and secondary properties such as R_e and M_* , which leads us in § 4.2 to discuss the fundamental plane relating BH mass and σ , R_e , and M_* . § 5 discusses the implications of this relation for predicting BH masses and demographics, and § 6 considers the physical origin of the BHFP relation. In § 7, we study how various theoretical quantities or initial conditions drive systems along the BHFP relation and, as a consequence, drive evolution in the various projections of the BHFP, and in § 8 apply this to understand the observed evolution with redshift in the $M_{\text{BH}} - M_*$ and $M_{\text{BH}} - \sigma$ relations. We summarize our

conclusions and discuss future tests of our proposed relations in § 9.

Throughout, we adopt a $\Omega_M = 0.3$, $\Omega_\Lambda = 0.7$, $H_0 = 70 \text{ km s}^{-1} \text{ Mpc}^{-1}$ cosmology (and correct all observations accordingly), but note this choice has little effect on our conclusions.

2. THE DATA

The observational data set with which we compare is described in detail in Paper I, but we summarize it here. We consider the sample of local BHs for which masses have been reliably determined via either kinematic or maser measurements. Specifically, we adopt the sample of 38 local systems for which values of M_{BH} , σ , R_e , M_{dyn} , and bulge luminosities are compiled in Marconi & Hunt (2003) and Häring & Rix (2004) (see also Magorrian et al. 1998; Merritt & Ferrarese 2001; Tremaine et al. 2002). We adopt the dynamical masses from the more detailed Jeans modeling in Häring & Rix (2004). We estimate the total stellar mass M_* from the total K -band luminosity given in Marconi & Hunt (2003), using the K -band mass-to-light ratios as a function of luminosity from Bell et al. (2003) (specifically assuming a “dwarf” Salpeter IMF, although this only affects the absolute normalization of the relevant relations). In Paper I it is also noted that the choice of these mass-to-light ratios as opposed to those determined from e.g. photometric fitting makes little difference. We take measurements of the Sersic index n_s from Graham & Driver (2006). Where possible, we update measurements of R_e , σ and n_s with more recent values from Lauer et al. (2005, 2006a); McDermid et al. (2006) and from Kormendy et al. (2007), which extends the baseline of surface brightness measurements allowing more robust estimates of n_s and R_e .

Although it should only affect the normalization of the relations herein, we note that our adopted cosmology is identical to that used to determine all quoted values in these works. The concentration index R_{30}/R_{50} for the observed systems is calculated assuming a Sersic profile with the best-fit n_s . When we fit the observations to e.g. the mean $M_{\text{BH}} - \sigma$ relation and other BH-host relations, we consider only the subsample of 27 objects in Marconi & Hunt (2003) which are deemed to have ‘secure’ BH and bulge measurements (i.e. for which the BH sphere of influence is clearly resolved, the bulge profile can be well-measured, and maser spots (where used to measure M_{BH}) are in Keplerian orbits). Our results are not qualitatively changed if we consider the entire sample in these fits, but their statistical significance is somewhat reduced.

3. SIMULATIONS

3.1. Methodology

Our simulations are taken from Robertson et al. (2006b), who utilize a set of several hundred simulations of major mergers to study the properties of remnants on the early-type galaxy FP. The properties of the models are discussed in detail therein, but we briefly review them here. The simulations were performed with the parallel TreeSPH code GADGET-2 (Springel 2005), based on a fully conservative formulation (Springel & Hernquist 2002) of smoothed particle hydrodynamics (SPH), which conserves energy and entropy simultaneously even when smoothing lengths evolve adaptively (see, e.g., Hernquist 1993; O’Shea et al. 2005). Our simulations account for radiative cooling, heating by a UV background (as in Katz et al. 1996; Davé et al. 1999), and in-

corporate a sub-resolution model of a multiphase interstellar medium (ISM) to describe star formation and supernova feedback (Springel & Hernquist 2003; Springel et al. 2005). Feedback from supernovae is captured in this sub-resolution model through an effective equation of state for star-forming gas, enabling us to stably evolve disks with arbitrary gas fractions (see Springel & Hernquist 2005; Robertson et al. 2006a). This feedback prescription can be adjusted between an isothermal gas with effective temperature of 10^4 K and our full multiphase model with an effective temperature $\sim 10^5$ K.

Supermassive black holes are represented by “sink” particles that accrete gas at a rate \dot{M} estimated from the local gas density and sound speed using an Eddington-limited prescription based on Bondi-Hoyle-Lyttleton accretion theory. The bolometric luminosity of the black hole is taken to be $L_{\text{bol}} = \epsilon_r \dot{M} c^2$, where $\epsilon_r = 0.1$ is the radiative efficiency. We assume that a small fraction (typically $\approx 5\%$) of L_{bol} couples dynamically to the surrounding gas, and that this feedback is injected into the gas as thermal energy, weighted by the SPH smoothing kernel. This fraction is a free parameter: we adjust it to match the normalization of the local $M_{\text{BH}} - \sigma$ relation as in Di Matteo et al. (2005, 2007); Sijacki et al. (2007). We emphasize that this controls only the normalization of this relation; i.e. inefficient feedback coupling means a BH must grow proportionally larger in order to couple the same energy to the ISM and self-regulate, but the scalings of BH mass with σ and host properties (i.e. slopes of the BH-host relations and correlations between residuals in these relations) are *not* changed. Because our comparisons throughout are based on the relative scalings of BH mass with host properties, this normalization choice is simply a matter of convenience. For now, we do not resolve the small-scale dynamics of the gas in the immediate vicinity of the black hole, but assume that the time-averaged accretion rate can be estimated from the gas properties on the scale of our spatial resolution (roughly ≈ 20 pc, in the best cases).

The progenitor galaxies in the mergers are constructed following Springel et al. (2005). For each simulation, we generate two stable, isolated disk galaxies, each with an extended dark matter halo with a Hernquist (1990) profile, motivated by cosmological simulations (e.g., Navarro et al. 1996; Busha et al. 2005), an exponential disk of gas and stars, and (optionally) a bulge. The galaxies have total masses $M_{\text{vir}} = V_{\text{vir}}^3 / (10G\bar{H}_0)$ for $z = 0$, with the baryonic disk having a mass fraction $m_d = 0.041$, the bulge (when present) having $m_b = 0.0136$, and the rest of the mass in dark matter. The dark matter halos are assigned a concentration parameter scaled as in Robertson et al. (2006c) appropriately for the galaxy mass and redshift following Bullock et al. (2001). The disk scale-length is computed based on an assumed spin parameter $\lambda = 0.033$, chosen to be near the mode in the λ distribution measured in simulations (Vitvitska et al. 2002), and the scale-length of the bulge is set to 0.2 times this.

Typically, each galaxy initially consists of 600,000 dark matter halo particles, 20,000 bulge particles (when present), 40,000 gas and 40,000 stellar disk particles, and one BH particle. We vary the numerical resolution, with many simulations using twice, and a subset up to 128 times, as many particles. We choose the initial seed mass of the black hole either in accord with the observed $M_{\text{BH}} - \sigma$ relation or to be sufficiently small that its presence will not have an immediate dynamical effect, but we have varied the seed mass to identify any systematic dependencies. Given the particle numbers employed,

the dark matter, gas, and star particles are all of roughly equal mass, and central cusps in the dark matter and bulge are reasonably well resolved (see Figure 2 in Springel et al. 2005).

We consider the set of several hundred simulations from Robertson et al. (2006b), in which we vary the numerical resolution, the orbit of the encounter (disk inclinations, pericenter separation), the masses and structural properties of the merging galaxies, initial gas fractions, halo concentrations, the parameters describing star formation and feedback from supernovae and black hole growth, and initial black hole masses. The detailed list of varied properties is given in Tables 1 & 2 of Robertson et al. (2006b). For example, the progenitor galaxies have virial velocities $V_{\text{vir}} = 50, 80, 115, 160, 226, 320$, and 500 km s^{-1} , and are constructed to match disks at redshifts $z = 0, 2, 3$, and 6 , and our simulations span a range in final black hole mass $M_{\text{BH}} \sim 10^5 - 10^{10} M_{\odot}$. The extensive range of conditions probed provides a large dynamic range, with final spheroid masses spanning $M_* \sim 10^8 - 10^{13} M_{\odot}$, covering the entire range of the observations we consider at all redshifts, and allows us to identify any systematic dependencies in our models. We consider initial disk gas fractions (by mass) of $f_{\text{gas}} = 0.05, 0.2, 0.4, 0.6, 0.8$, and 1.0 for several choices of virial velocities, redshifts, and ISM equations of state.

The results described in this paper are based primarily on simulations of equal-mass mergers; however, by examining a small set of simulations of unequal mass mergers, we find that the behavior does not change significantly for mass ratios down to about 1:3 or 1:4, below which mass ratio the mergers produce neither substantial BH nor bulge growth, and therefore are no longer appropriate to compare to local relations between BHs and massive spheroids.

3.2. Analysis

Each simulation is evolved until the merger is complete and the remnants are fully relaxed, typically $\sim 1 - 2$ Gyr after the final merger and coalescence of the BHs. We then measure kinematic properties of the remnants following Robertson et al. (2006b); Cox et al. (2006b). The effective radius R_e is the projected half-mass stellar effective radius, and the velocity dispersion σ is the average one-dimensional velocity dispersion within a circular aperture of radius R_e . Projected quantities such as R_e , σ , and the stellar surface mass density $I_e \equiv M_*(r < R_e) / \pi R_e^2$ are averaged over 100 random lines of sight to the remnant. Throughout, the stellar mass M_* refers to the total stellar mass of the galaxy, and the dynamical mass M_{dyn} refers to the traditional dynamical mass estimator

$$M_{\text{dyn}} \equiv k \frac{\sigma^2 R_e}{G}, \quad (1)$$

where we adopt $k = 8/3$ (although this choice is irrelevant as long as we apply it uniformly to both observations and simulations). We define ϕ_c as the gravitational potential from the galaxy (excluding the BH itself) at the location of the BH (given the typical resolution over which this quantity is smoothed, this is effectively the converged bulge potential at $r = 0$, in the absence of the BH; see Springel 2005). As a concentration index we adopt the ratio of half-mass radius $R_e = R_{50}$ to 30%-mass radius R_{30} , and measure n_s from projected mock images following Krause et al. (2007, in preparation). We note that, for convenience, f_{gas} typically refers to the gas fraction in the merging disks when the simulations are initialized, but show in § 7 that our results are unchanged (al-

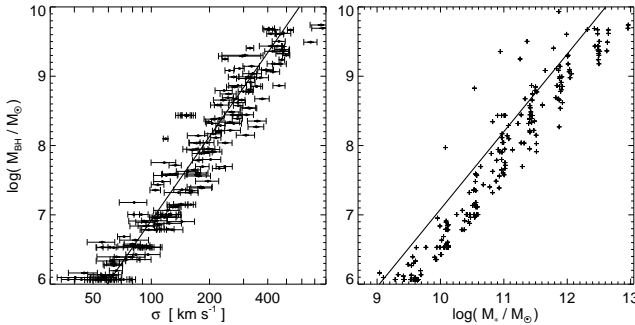


FIG. 1.— Location of our simulation merger remnant spheroids on the $M_{\text{BH}} - \sigma$ and $M_{\text{BH}} - M_*$ relations (as in Di Matteo et al. 2005; Robertson et al. 2006c). Solid lines show the observed relations from Tremaine et al. (2002) and Häring & Rix (2004). Error bars in σ show the dispersion across 100 random viewing angles. The simulations reproduce well the observed relations over a wide dynamic range. As discussed in the text, there are a number of likely reasons for the slight (0.2dex) normalization offset in M_* , but insofar as the slopes of the relations are identical, this has no effect on our analysis.

though f_{gas} itself systematically shifts) regardless of the time before the merger at which we choose to define the gas fraction of the systems.

4. THE LOCAL BH-HOST CORRELATIONS

4.1. One-to-One Relationships

Figure 1 shows the location of our simulation remnants on the the $M_{\text{BH}} - \sigma$ and $M_{\text{BH}} - M_*$ relations. As demonstrated by Di Matteo et al. (2005), they agree well with the observed relations over a large dynamic range. Critically, although modifying our feedback prescriptions and, as we show below, adjusting the kinematic properties of the remnants by changing e.g. orbital parameters and gas fractions of the merging systems can shift the normalization of the relations, the slopes are *not* adjustable or tunable, but are a natural consequence of self-regulated BH growth. We note that there is a slight offset between the normalization (but not slope) of our predicted $M_{\text{BH}} - M_*$ relation and that measured by Häring & Rix (2004), but a weaker offset in $M_{\text{BH}} - \sigma$. This owes to the fact that, at fixed σ , our simulated systems typically have slightly larger (mean offset ≈ 0.16 dex) stellar masses than the observed systems on the $M_{\text{BH}} - \sigma$ relation. There are a number of possible explanations for this offset in the Faber-Jackson ($M_*[\sigma]$) relation. As pointed out by Bernardi et al. (2006), the systems with measured BH masses in Häring & Rix (2004) actually lie above the Faber-Jackson relation observed for typical early-type galaxies, perhaps owing to a selection bias. Their estimate of the magnitude of this bias is quite similar to the offset here and can completely account for our results.

Furthermore, we show below that at fixed M_* , changing the gas fractions of the merging systems, their orbits, or their structural properties can systematically drive changes in σ . This means that the precise normalization of the observed Faber-Jackson relation depends, in detail, on the exact star formation and merger histories of the systems observed. Since we do not model these cosmological histories, but rather isolate different mergers in order to study how these changes are driven, it is not surprising that the normalizations of the relations do not happen to match perfectly. In any case, we are interested in how offsets or evolution from one relation or the other are produced, and how such residuals may scale with other host properties, for which the actual normalization of the relation factors out completely. It therefore makes no difference to our analysis (although we have considered both

cases) whether we compare to our full suite or select only a subset of simulations which reproduce the (mean) normalization in the observed Faber-Jackson relation.

Figure 2 shows the correlation between BH mass and a wide variety of host properties, from both our simulations and the observed sample. The slopes of the simulated correlations are essentially identical to those observed in every case. Note that many of the correlations are similarly tight, including the correlations with velocity dispersion σ , stellar mass M_* , dynamical mass M_{dyn} , effective bulge binding energy $M_* \sigma^2$, and central potential ϕ_c . The best-fit correlations are listed in Table 1, along with the intrinsic scatter in M_{BH} estimated about each correlation from the simulations. We do not list the correlation with M_{halo} , as it is clear in our simulations that BH mass is correlated with small-scale bulge properties (unsurprising, given that the central potential of the bulge is strongly baryon-dominated). Therefore, while there is an indirect correlation with M_{halo} through e.g. the $M_{\text{halo}} - M_*$ and $M_{\text{BH}} - M_*$ relations, its nature depends systematically on the exact $M_{\text{halo}} - M_*$ relation.

We also note that the (relatively large) scatter in the correlations between M_{BH} and concentration or Sersic index in Figure 2 appears contrary to the conclusions of Graham et al. (2001), who argue for very small intrinsic scatter in these correlations. However, Novak et al. (2006) point out that uncertainty in this correlation, unlike for the $M_{\text{BH}} - \sigma$ or $M_{\text{BH}} - M_{\text{dyn}}$ relations, is dominated by the measurement errors in concentration index or n_s , which means that improved observations are needed to determine whether the relation is actually consistent with small intrinsic scatter. In fact, when we update the measurements from Graham et al. (2001) and Graham & Driver (2006) with the n_s measurements from Kormendy et al. (2007), which typically reduce the measurement error in n_s from $\sim 20\%$ to $< 5\%$ (and in at least two cases⁴ change n_s by $> 3\sigma$ relative to the Graham & Driver (2006) fit), the quality of the correlation is substantially degraded, and a significantly larger intrinsic scatter is implied.

In the simulations, it is possible, given appropriate gas fractions or orbital parameters, to substantially change n_s or R_{30}/R_{50} at fixed stellar mass without driving a corresponding change in M_{BH} (n_s also appears to be more variable sightline-to-sightline than other projected quantities such as σ or R_e). As will be discussed in detail in Krause et al. (2007, in preparation), this has the consequence that the values of n_s predicted by a uniform set of simulations are not as tightly correlated with spheroid mass as is observed (and, as a secondary consequence, M_{BH} , which is tightly correlated with M_* , is less well-correlated with n_s). Furthermore, the weaker correlation in the simulations should not be surprising – unlike the $M_* - R_e$ or $M_* - \sigma$ correlations which are produced fundamentally (at least to lowest order) by basic dynamical effects (and are not especially sensitive to the exact type of spheroid-producing mergers), it is commonly believed (e.g., Kormendy et al. 2007) that the correlation between n_s and M_* is driven by an increasing prevalence of dissipationless (spheroid-spheroid) mergers at higher masses. Such mergers will, by definition, conserve the $M_{\text{BH}} - M_*$ relation, but simulations have shown that they dramatically change n_s (e.g.

⁴ Graham & Driver (2006) quote $n_s = 3.04^{+0.61}_{-0.51}$, $2.73^{+0.55}_{-0.46}$, for NGC 3377 and 4473, respectively, whereas Kormendy et al. (2007) measure $n_s = 4.917$, 6.04 ± 0.33 . The newer values make the measured M_{BH} discrepant with the $M_{\text{BH}} - n_s$ relation in Graham & Driver (2006) by 0.64 and 0.78 dex, respectively (with ≈ 0.15 dex measurement errors in M_{BH} for each).

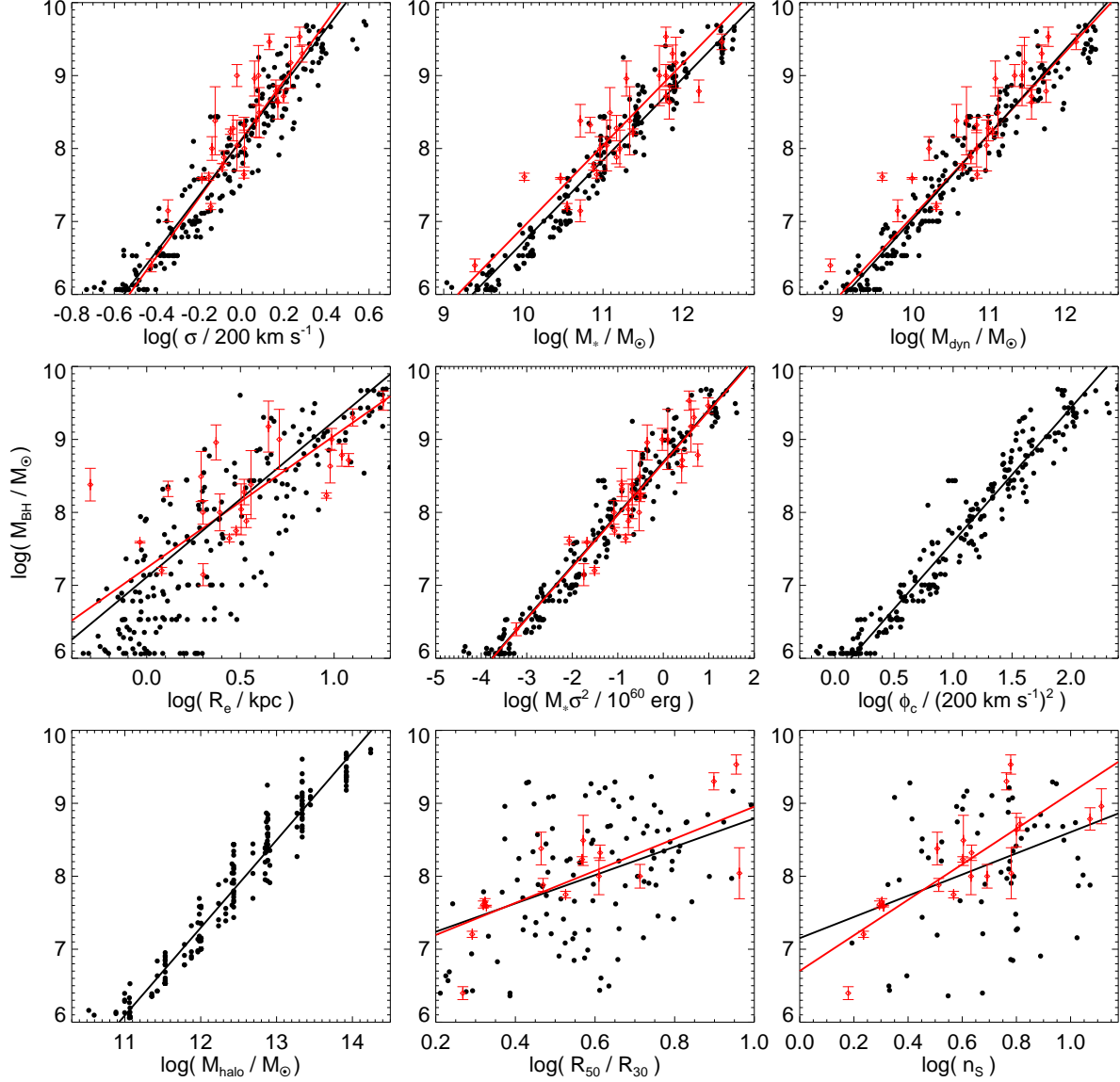


FIG. 2.— Correlations between BH mass and a variety of host spheroid properties. Red points with error bars are the observations; red line shows the least-squares best-fit to each relation. Note that the quality of the correlation between M_{BH} and concentration or Sersic index observed is significantly reduced relative to that in Graham et al. (2001); Graham & Driver (2006) when we adopt the Sersic index measurements from Kormendy et al. (2007). Black points and lines are the results of hydrodynamic simulations (see § 3). The slopes of the simulated and observed relations are statistically identical in every case, with all normalization offsets owing to the small Faber-Jackson ($M_*(\sigma)$) offset in Figure 1.

Boylan-Kolchin et al. 2006) and therefore the $M_{\text{BH}} - n_s$ relation. If this is true, then the $M_{\text{BH}} - n_s$ correlation, unlike the $M_{\text{BH}} - M_*$ relation, must fundamentally be driven by cosmological effects (e.g. the differential contribution of different merger types as a function of mass and redshift), which our simulations do not represent. A more accurate modeling is outside the scope of this paper, as it would require a fully cosmological prediction for merger rates (as a function of type, mass, and redshift) with high-resolution cosmological simulations such that the central galaxy structure and BH feedback effects could be modeled. The $M_{\text{BH}} - M_*$ and BHFP relations on which we focus, on the other hand, should be relatively robust to these effects (see also § 9).

4.2. A Black Hole Fundamental Plane

We wish to determine whether or not a simple one-to-one correlation between e.g. M_{BH} and σ is a sufficient descrip-

tion of the simulations, or whether there is evidence for additional dependence on a second parameter such as R_e or M_* . The most efficient way to determine such a dependence is by looking for correlations between the residuals of the various projections of such a potential BHFP relation. Following Paper I, Figure 3 plots the correlation between BH mass M_{BH} and host bulge effective radius R_e at fixed σ . Specifically, we determine the residual with respect to the $M_{\text{BH}} - \sigma$ relation by fitting $M_{\text{BH}}(\sigma)$ to an arbitrary log-polynomial

$$\langle \log(M_{\text{BH}}) \rangle = \sum [a_n \log(\sigma)^n], \quad (2)$$

allowing as many terms as the data favor (i.e. until $\Delta\chi^2$ with respect to the fitted relation is < 1), and then taking

$$\Delta \log(M_{\text{BH}} | \sigma) \equiv \log(M_{\text{BH}}) - \langle \log(M_{\text{BH}}) \rangle(\sigma). \quad (3)$$

We determine the residual $\Delta \log(R_e | \sigma)$ (or $\Delta \log(R_e | \sigma)$, for the stellar mass) in identical fashion, and plot the correlation

TABLE 1
BH-HOST CORRELATIONS

Variables ^{1,5}	Observed			Simulated		
	Normalization ²	Slope ³	Scatter ⁴	Normalization	Slope ³	Scatter
$\sigma^\alpha R_e^\beta$	8.33 ± 0.06	$3.00 \pm 0.30, 0.43 \pm 0.19$	0.21	8.16 ± 0.05	$2.90 \pm 0.38, 0.54 \pm 0.11$	0.21
$M_*^\alpha \sigma^\beta$	8.24 ± 0.06	$0.54 \pm 0.17, 2.18 \pm 0.58$	0.22	7.93 ± 0.06	$0.72 \pm 0.12, 1.40 \pm 0.49$	0.19
$M_*^\alpha R_e^\beta$	8.06 ± 0.07	$1.78 \pm 0.40, -1.05 \pm 0.37$	0.25	7.64 ± 0.04	$1.50 \pm 0.22, -0.56 \pm 0.26$	0.21
$M_* \sigma^2$	8.23 ± 0.06	0.71 ± 0.06	0.25	7.92 ± 0.04	0.71 ± 0.03	0.21
σ	8.28 ± 0.08	3.96 ± 0.39	0.31	8.04 ± 0.06	3.91 ± 0.20	0.31
M_*	8.21 ± 0.07	0.98 ± 0.10	0.33	7.85 ± 0.05	1.16 ± 0.06	0.23
M_{dyn}	8.22 ± 0.10	1.05 ± 0.13	0.43	8.18 ± 0.06	1.05 ± 0.06	0.28
R_e	8.44 ± 0.10	1.33 ± 0.25	0.45	8.48 ± 0.12	1.92 ± 0.14	0.56
ϕ_c	–	–	–	8.31 ± 0.05	1.77 ± 0.08	0.23

¹ For the variables (x, y) , a correlation of the form $\log(M_{\text{BH}}) = \alpha \log(x) + \beta \log(y) + \delta$ is assumed, where the normalization is δ and α, β are the logarithmic slopes.

² The normalization gives $\log(M_{\text{BH}}/M_\odot)$ for $\sigma = 200 \text{ km s}^{-1}$, $M_* = 10^{11} M_\odot$, $M_{\text{dyn}} = 10^{11} M_\odot$, $R_e = 5 \text{ kpc}$, which roughly minimizes the covariance between fit parameters.

³ Errors quoted here for the BHFP relations in (σ, R_e) , (M_*, σ) , and (M_*, R_e) include the covariance between the two slopes. Holding one of the two fixed and varying the other yields substantially smaller errors (typically $\sim 5\%$). All quoted errors account for measurement errors in both M_{BH} and the relevant independent variables.

⁴ The internal scatter is estimated from both the simulations and observations as that which yields a reduced $\chi^2/\nu = 1$ with respect to the given best-fit relation.

⁵ Central potential ϕ_c , normalization at $\phi_c = 10^6 \text{ km}^2 \text{ s}^{-2}$. There are no observational measurements presently available to compare with this correlation.

between the two. We allow arbitrarily high terms in $\log(\sigma)$ to avoid introducing bias by assuming e.g. a simple power-law correlation between M_{BH} and σ , but find in practice that such terms are not needed – as discussed in Paper I, there is no significant evidence for a log-quadratic (or higher-order) dependence of M_{BH} on σ , R_e , or M_* , so allowing for these terms changes the residual best-fit solutions by $\ll 1\sigma$. Of course, even this approach could in principle introduce a bias via our assumption of some functional form, and so we have also considered a non-parametric approach where we take the mean $\langle \log(M_{\text{BH}}) \rangle$ in bins of $\log(\sigma)$. Our large set of simulations allows us to do this with very narrow binning, and we recover a nearly identical answer.

The simulations show a highly significant correlation between M_{BH} and R_e at fixed σ , similar to the observed trend in residuals. We therefore introduce a FP-like relation of the form

$$M_{\text{BH}} \propto \sigma^\alpha R_e^\beta, \quad (4)$$

which can account for these dependencies. Formally, we determine the combination of (α, β) which simultaneously minimizes the χ^2/ν of the fit and the significance of the correlations between the residuals in σ and M_{BH} (or R_e and M_{BH}). This yields similar results to the direct fitting method of Bernardi et al. (2003b) from the spheroid FP, which minimizes

$$\Delta^2 = [\log(M_{\text{BH}}) - \alpha \log(\sigma) - \beta \log(R_e) - \delta]^2, \quad (5)$$

and corresponds exactly to the method used in fitting the observations in Paper I, to which we compare. This yields a best-fit BHFP relation

$$\log(M_{\text{BH}}) = 8.16 + 2.90(\pm 0.38) \log(\sigma/200 \text{ km s}^{-1}) \quad (6)$$

$$+ 0.54(\pm 0.11) \log(R_e/5 \text{ kpc})$$

from the simulations, similar to the observed BHFP relation, $M_{\text{BH}} \propto \sigma^{3.0 \pm 0.3} R_e^{0.43 \pm 0.19}$ (Paper I). Unsurprisingly, the slopes in the BHFP relation are close to those formally determined for the residuals in Figure 3. Figure 4 plots the residuals of M_{BH} with respect to these fundamental plane relations, at fixed R_e and fixed σ . The introduction of a BHFP eliminates the strong systematic correlations between the residuals, yielding flat errors as a function of σ and R_e .

Given the definition of $M_{\text{dyn}} \propto \sigma^2 R_e$, it is trivial to convert the best-fit BHFP relation in terms of σ and R_e to one in M_{dyn} , obtaining

$$\begin{aligned} \log(M_{\text{BH}}) &= 8.11 + 0.54 \log(M_{\text{dyn}}/10^{11} M_\odot) & (7) \\ &+ 1.82 \log(\sigma/200 \text{ km s}^{-1}) \\ &= 8.03 + 1.45 \log(M_{\text{dyn}}/10^{11} M_\odot) \\ &- 0.91 \log(R_e/5 \text{ kpc}). \end{aligned}$$

As is the case for the observed systems, the correlation with either σ or R_e at fixed M_{dyn} is non-zero and highly significant (i.e. the BHFP is not simply a reflection of a simpler $M_{\text{BH}} - M_{\text{dyn}}$ relation).

At low redshift, σ , R_e , and M_{dyn} can be determined reliably, but at high redshift it is typically the stellar mass M_* or luminosity which is used to estimate M_{BH} . Therefore, it is interesting to examine the BHFP projections in terms of e.g. M_* and σ or M_* and R_e . Repeating our analysis, we find in Figures 5 & 6 that the observations demand a FP relation over a simple $M_{\text{BH}}(M_*)$ relation at high significance. We find a nearly identical result using the dynamical mass, $M_{\text{dyn}} \propto \sigma^2 R_e$, instead of stellar mass M_* , as expected from the BHFP in terms of σ and R_e . The exact values of the best-fit coefficients of this BHFP

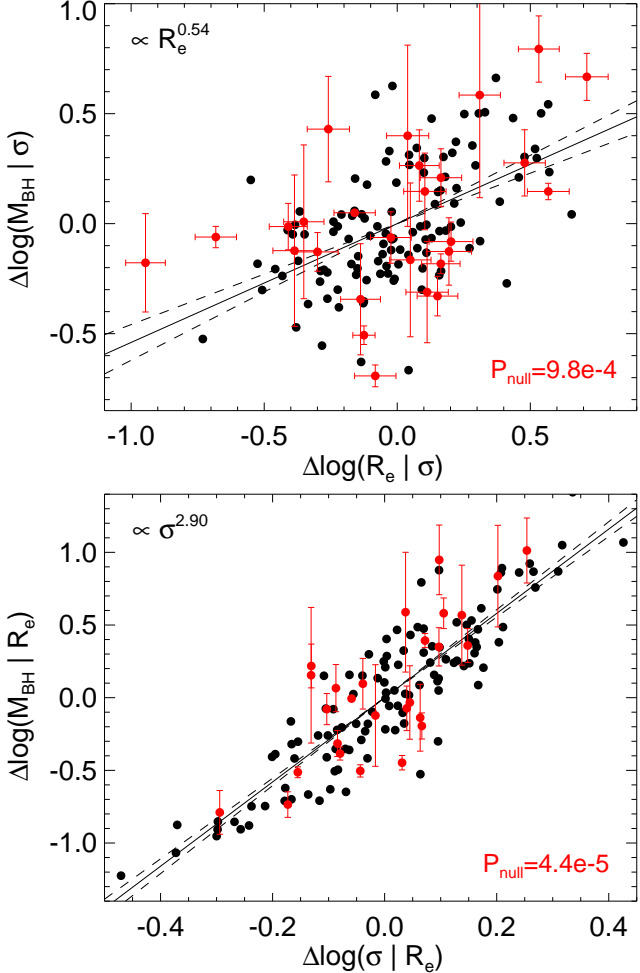


FIG. 3.— *Upper:* Correlation between the residuals in the $M_{\text{BH}} - \sigma$ relation and $R_e - \sigma$ relation, from our simulations (black points) and observed sample (red points with errors). At fixed σ , systems with larger effective radii R_e also have larger black hole masses M_{BH} . The fit to this residual correlation is shown with the black lines ($\pm 1\sigma$ range in the best-fit correlation shown as dashed lines – note that they are strongly inconsistent with zero correlation), with the slope shown. The probability of the null hypothesis of no correlation in the residuals (i.e. no systematic dependence of M_{BH} on R_e at fixed σ) for the observed systems is shown (red P_{null}) – the observations imply a secondary “fundamental plane”-type correlation at 3σ . *Lower:* Same, but considering the correlation between M_{BH} and σ at fixed effective radius R_e .

determined from the observations are given (along with those of various other BHFP projections) in Table 1.

Because the simulation merger remnant spheroids lie on a stellar-mass fundamental plane very similar to observed elliptical galaxies (Robertson et al. 2006b), which tightly relates M_* , R_e , and σ , the BHFP in terms of any two of those variables can be easily converted to any other two. In other words, the two forms of the BHFP ($M_{\text{BH}} \propto \sigma^3 R_e^{1/2}$ and $M_{\text{BH}} \propto \sigma^2 M_*^{1/2}$) are completely equivalent (the choice between them is purely a matter of convenience), and it is redundant to search for a four-variable correlation (of the form $M_{\text{BH}} \propto \sigma^\alpha R_e^\beta M_*^\gamma$). As in the case of the observations (Paper I), we stress that no transformation (given the early-type FP relating these three variables) eliminates the dependence on two variables – i.e. no transformation from any one BHFP allows us to write M_{BH} as a pure function of either σ , R_e , M_* , or M_{dyn} .

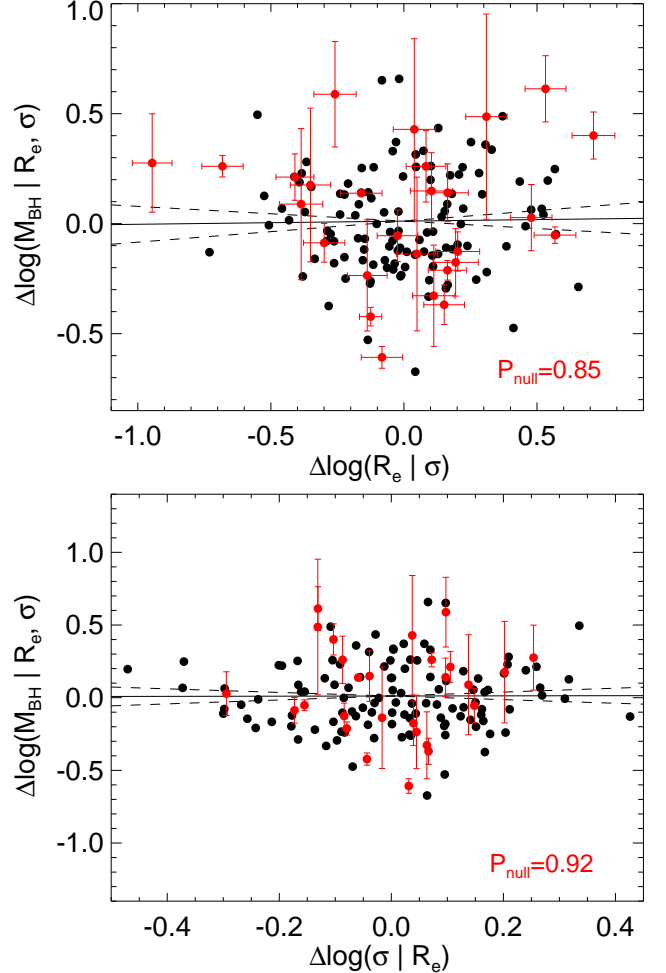


FIG. 4.— Correlation between the residuals in our BH “fundamental plane” relation $M_{\text{BH}} \propto \sigma^{2.90} R_e^{0.54}$ and effective radius R_e at fixed σ (*upper*) or σ at fixed R_e (*lower*). Accounting for the joint dependence of M_{BH} on σ and R_e removes the strong systematic dependencies in the residuals from Figure 3 (P_{null} is large, meaning there is no further residual dependence).

5. IMPLICATIONS OF THE BHFP FOR LOCAL BH MASSES AND DEMOGRAPHICS

Given that the “true” correlation between M_{BH} and host properties appears to follow a FP-like relation, it is natural to ask how adopting such a relation affects the estimation of BH masses from observed host properties. Figure 7 shows the observed and simulated systems in the fundamental plane. The relation appears to be a good predictor of M_{BH} over a large dynamic range, and there is no evidence for any curvature or higher-order terms in the relation (fitting e.g. a log-quadratic relation in this space yields $\Delta\chi^2 < 1$). As detailed in Table 1, the intrinsic scatter in the BHFP is small, typically ~ 0.2 dex, and in all cases smaller than the scatter in e.g. the $M_{\text{BH}} - \sigma$ or $M_{\text{BH}} - M_*$ relations.

However, as Novak et al. (2006) note, minimizing the intrinsic scatter does not necessarily maximize the observational ability to predict BH masses. The BHFP relations depend on measuring two of either σ , R_e , or M_* , and therefore introduce additional errors from the measurements of two (as opposed to just one) of these quantities. At low redshifts, it may be possible to obtain accurate measurements of both σ and R_e and therefore still obtain more accurate mass estimates (although we caution that several of the literature sources from

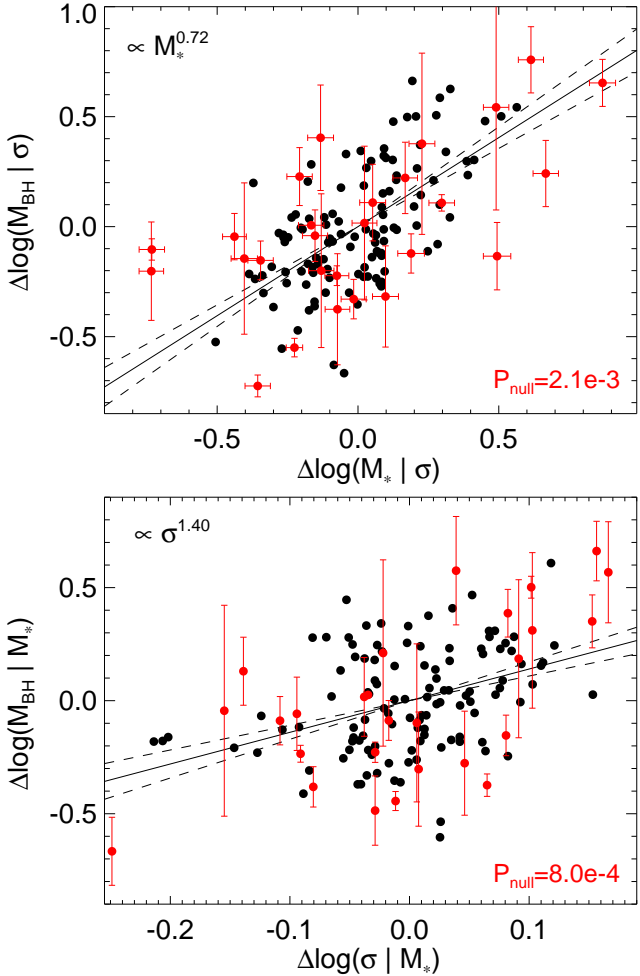


FIG. 5.— As Figure 3, but considering the correlation between the residual in BH mass M_{BH} and stellar mass M_* at fixed velocity dispersion σ (upper), or between M_{BH} and σ at fixed M_* (lower). Observed and simulated systems with larger velocity dispersions (deeper potential wells) at fixed stellar mass have more massive BHs, as do more massive systems at fixed σ . A nearly identical result is obtained using dynamical mass M_{dyn} instead of stellar mass M_* : a residual dependence $\propto M_{\text{dyn}}^{0.55 \pm 0.09}$ ($P_{\text{null}} = 0.0037$) at fixed σ and $\propto \sigma^{2.16 \pm 0.79}$ ($P_{\text{null}} = 0.0032$) at fixed M_{dyn} .

which we compile observations differ by $> 2\sigma$ in some R_e measurements, owing to various systematic issues such as the choice of observed bands). However, at high redshifts M_* remains the most easily applicable proxy for M_{BH} , and it is not clear that the additional accuracy gained by introducing the R_e term substantially improves the predictive power of the relation.

Ultimately, the $M_{\text{BH}} - \sigma$ and $M_{\text{BH}} - M_*$ relations are not much worse in a mean sense around $M_{\text{BH}} \sim 10^8 - 10^9 M_\odot$, with relatively small intrinsic scatter (see Table 1). The reason these relations work as well as they do is that they are both nearly edge-on projections of the BHFP. Given a relation $M_{\text{BH}} \propto \sigma^3 R_e^{0.5}$, it is not surprising that σ is an acceptable proxy for M_{BH} in many situations (whereas the $M_{\text{BH}} - R_e$ correlation has quite large scatter, as R_e enters with a relatively weak dependence in the BHFP).

However, given that there is a systematic dependence on e.g. M_* or R_e at fixed σ which is captured only by the BHFP relations, we expect that the importance of estimating BH masses from the BHFP will be enhanced at the ex-

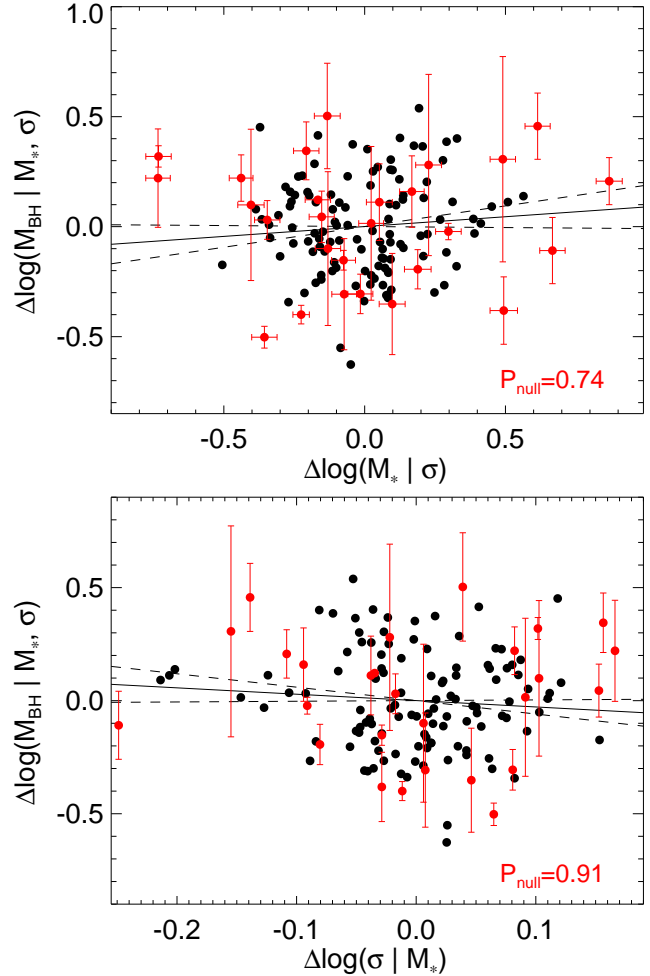


FIG. 6.— As Figure 4, but considering the residuals with respect to the BHFP defined in terms of stellar mass and σ . Placing the simulations and observations in the context of a FP relation eliminates the strong trends in their residuals.

tremes of observed distributions. Figure 8 compares the locations of outliers in the simulated and observed $M_{\text{BH}} - \sigma$ and $M_{\text{BH}} - M_{\text{dyn}}$ relations with their locations on the BHFP relations. Indeed, several systems which appear as outliers in one of the projections of the BHFP are no longer significant outliers in the BHFP relation. This is true for a number of systems on both the $M_{\text{BH}} - M_*$ relation and the $M_{\text{BH}} - \sigma$ relation⁵. These systems typically have abnormally high or low velocity dispersions given their stellar mass, and therefore appear deviant in the BHFP projections, just as such systems typically appear to deviate from the spheroid FP in projections such as the $R_e - M_*$ or Faber-Jackson ($M_* - \sigma$) relations. Therefore, while the typical scatter about the mean relation is not dramatically different for the BHFP (~ 0.2 dex) compared to the $M_{\text{BH}} - \sigma$ relation (~ 0.3 dex), the tails of this distribution are substantially suppressed when we adopt the BHFP as a BH mass estimator.

Given the potential importance of the BHFP for predicting the masses of BHs, especially in extreme systems, we should examine the implications that the relation has for

⁵ NGC 1023, 3384, 4697, 5252, and Cygnus A have BH mass measurement errors of < 0.1 dex and measured masses which are 0.32, 0.96, 0.81, 0.53, and 0.34 dex discrepant with the expectation from the Tremaine et al. (2002) relation, but only 0.10, 0.70, 0.51, 0.44, and 0.23 dex discrepant with the BHFP expectation, respectively.

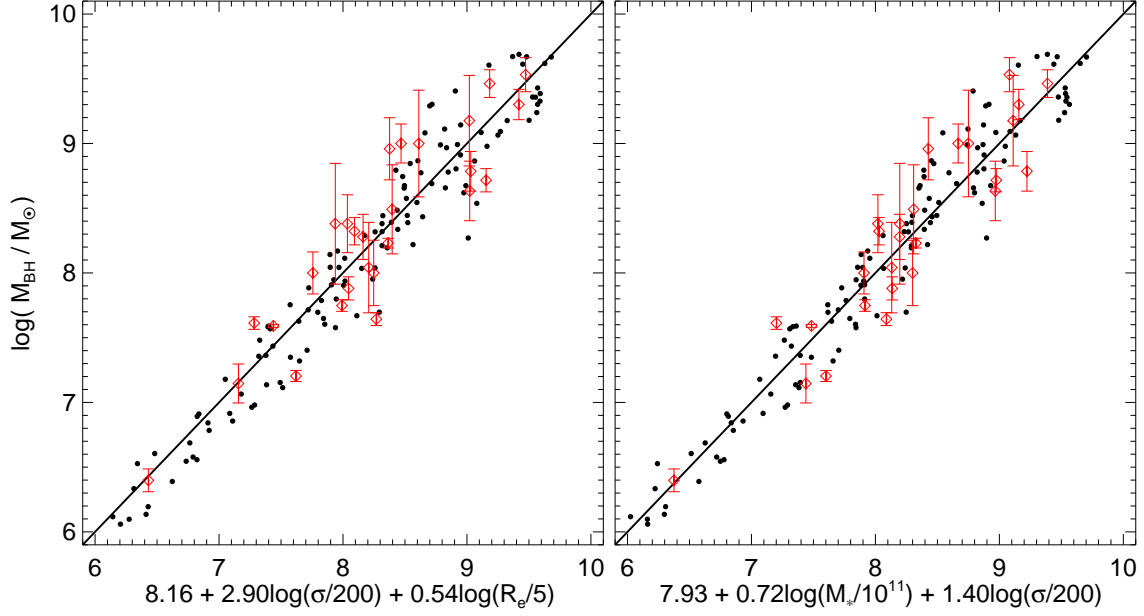


FIG. 7.— Masses of BHs in our simulations and from local measurements, compared to the expectation from the best-fit BHFP relations in σ , R_e and M_* , σ . The two agree well at all masses, without any evidence for curvature in the relations. The intrinsic scatter in M_{BH} at fixed σ , R_e or M_* , σ is estimated from the simulations to be ≈ 0.20 dex (see Table 1), which is consistent with the scatter in the observed points (given their measurement errors).

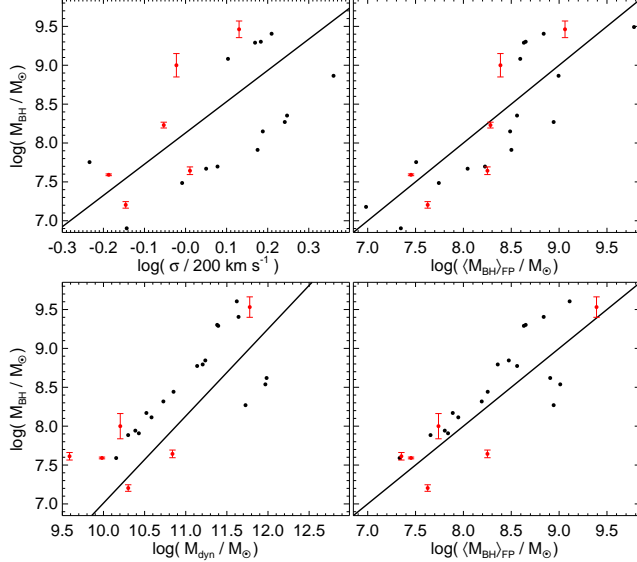


FIG. 8.— *Upper:* Outliers in the local $M_{\text{BH}} - \sigma$ relation from the observations (red; defined as points $> 3\sigma$ discrepant from the mean trend) and simulations (black; defined as points 0.5dex discrepant from the mean trend) are plotted relative to the mean relation from Tremaine et al. (2002) (line) (*left*), and plotted relative to the expected BH mass from the fundamental plane relation (*right*). *Lower:* Same, but for outliers from the local $M_{\text{BH}} - M_{\text{dyn}}$ relation from Härting & Rix (2004). Most outliers in $M_{\text{BH}} - \sigma$ or $M_{\text{BH}} - M_{\text{dyn}}$ are explained by the BHFP relations we derive – i.e. they have abnormal values of σ or R_e for their masses, but are not outliers in the BHFP relation. There are a small number of observed and simulated systems which are genuine outliers from all relations – i.e. do have anomalous BH masses, but we note that there are no simulated or observed systems that are outliers from the BHFP relations and *not* also outliers from $M_{\text{BH}} - \sigma$ or $M_{\text{BH}} - M_{\text{dyn}}$.

the local demographics of BHs. There has been substantial debate recently about whether or not high- M_* systems begin to deviate from the low- M_* Faber-Jackson relation (see, e.g. Boylan-Kolchin et al. 2006; Bernardi et al. 2006; Batcheldor et al. 2006). If so, this implies that either the $M_{\text{BH}} - M_*$ or $M_{\text{BH}} - \sigma$ relation must change slope at the high-

est masses, with one of the two or some other relation being the conserved relation. Because the distribution of spheroid velocity dispersions (Sheth et al. 2003) declines more steeply at high σ than the galaxy mass or luminosity functions do at high M_* (when BCGs are included), the assumption that the $M_{\text{BH}} - M_*$ relation remains unchanged (the simplest expectation from gas-free or “dry” mergers) naively predicts a much higher abundance of very high-mass ($\gtrsim 10^9 M_{\odot}$) BHs (for an extended discussion, see Lauer et al. 2006b).

Figure 9 compares the expected BH mass function (BHMF) from the observed distribution of spheroid velocity dispersions and the $M_{\text{BH}} - \sigma$ relation with that expected from the early-type galaxy stellar mass function and the $M_{\text{BH}} - M_*$ relation. We adopt the distribution of velocity dispersions σ from Sheth et al. (2003), and the early-type galaxy stellar mass function from Bell et al. (2003), with the addition of BCGs at high masses from Lin & Mohr (2004) (yielding a shallower power law-like falloff at high masses, as opposed to an exponential cutoff). Note that a similar result is obtained estimating the BCG mass function from Lauer et al. (2006b) or using the Cole et al. (2001) or Jones et al. (2006) K -band luminosity functions from the 2dF and 6dF respectively (converted to mass functions following Bell et al. (2003)), which include BCGs and extend to the low space densities of interest. (In any case we are simply attempting to highlight the key qualitative behavior, that with the inclusion of BCGs the stellar mass function falls off more slowly than the velocity dispersion function.)

For now, we assume a one-to-one correlation between M_{BH} and σ or M_* . Given this, there would also be a one-to-one correlation between M_* and σ (i.e. $\sigma(M_*)$ is given by matching the two distributions at fixed number density), so we can use the BHFP relation in the form $M_{\text{BH}} \propto M_*^\alpha \sigma^\beta$ to estimate the BHMF from this relation. Unsurprisingly, we find that the BHMF from $M_{\text{BH}} - \sigma$ cuts off rapidly compared to that from $M_{\text{BH}} - M_*$. With a mixed dependence on both σ and M_* , the BHFP relation predicts a somewhat intermediate case at high masses, although it is closer to the expectation from

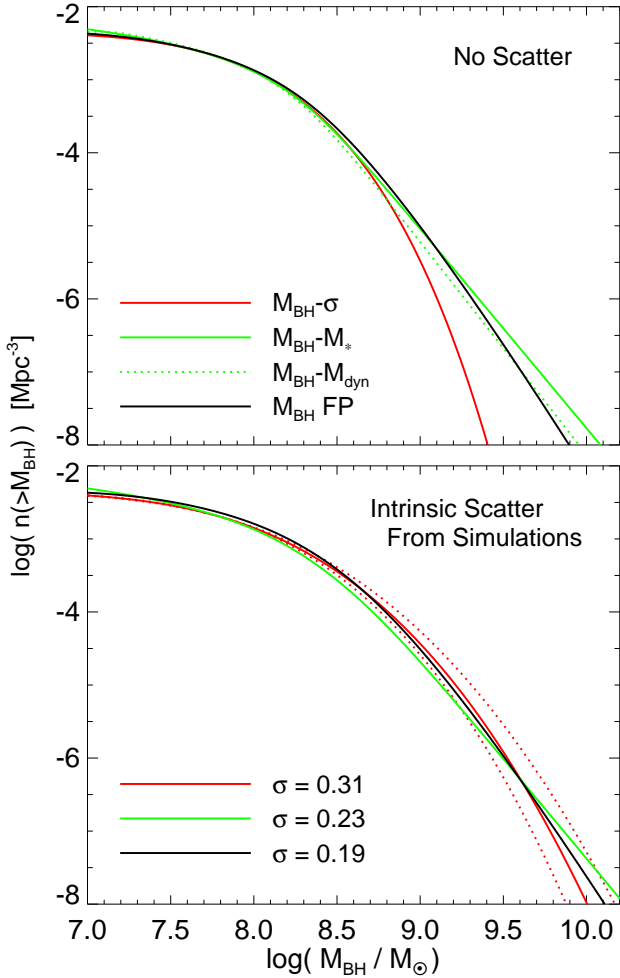


FIG. 9.— BH mass function (cumulative number density above a given mass) expected from the observed early-type velocity dispersion function (with the $M_{\text{BH}} - \sigma$ relation from Tremaine et al. (2002)), the observed early-type stellar mass function (with the $M_{\text{BH}} - M_*$ relation herein, but this is quite similar to the $M_{\text{BH}} - M_{\text{dyn}}$ relation from Häring & Rix (2004)), and from the joint distribution of M_* and σ (given the observed $M_* - \sigma$ relations from Bernardi et al. (2003a) or implied by the two distribution functions, and our BHFP relation) or σ and R_e (with the observed $M_{\text{BH}} - M_{\text{dyn}}$ relation). The implied BHMF at high masses is very different for some of the various correlations, if we ignore the scatter in the relations (*upper*), with the BHFP representing an intermediate case (albeit closer to $M_{\text{BH}} - M_*$ than $M_{\text{BH}} - \sigma$). However, accounting for the intrinsic scatter in each correlation estimated from our simulations (*lower*) yields nearly identical BHMFs even at $\sim 10^{10} M_\odot$. Larger scatter in the $M_{\text{BH}} - \sigma$ relation at high masses reflects (and compensates for) the discrepancy at high- M_{BH} . Dotted lines show the BHMF inferred from $M_{\text{BH}} - \sigma$ with a change of just 25% in the estimated intrinsic scatter (from a scatter of $\sigma = 0.31$ to $\sigma = 0.27, 0.36$), which demonstrates that a small uncertainty in the intrinsic scatter (difficult to determine observationally) can dominate the choice of BH-host correlation adopted, even at very high M_{BH} .

$M_{\text{BH}} - M_*$.

However, this treatment ignores the important fact that there is scatter in these correlations. To predict the BHMF from the distribution of velocity dispersions, we should properly convolve over the mean relation broadened by some (approximately lognormal) dispersion with width ~ 0.3 dex. The intrinsic scatter is difficult to determine from the observations, if errors are not completely understood, so we adopt the intrinsic scatter in each correlation estimated from our simulations (Table 1). Given this scatter, we re-calculate the expected BHMFs, shown in Figure 9. Interestingly, the three predicted BHMFs are now almost identical, even at very high

BH masses ($\gtrsim 5 \times 10^9$). This is expected – if we completely understand the correlation (and its scatter) between M_{BH} and either σ or M_* over the entire mass range of interest, then any projected version of the same BHFP must yield a similar BHMF. The fact that the distribution of σ cuts off more steeply than M_* is compensated by the fact that the intrinsic scatter in $M_{\text{BH}} - \sigma$ is slightly larger than in $M_{\text{BH}} - M_*$ (see also Marconi et al. 2004). This is roughly equivalent to the statement that at large masses, where the relation between σ and M_* may change, the $M_{\text{BH}} - \sigma$ relation must change correspondingly (following the true BHFP relation; for a more detailed comparison see Lauer et al. 2006b). Because the distribution of σ falls rapidly at high σ , there is little contribution at low- M_{BH} from high- σ systems, so a change in slope or increase in scatter in $M_{\text{BH}} - \sigma$ both have the primary effect of increasing the expected number of high-mass BHs, reconciling the BHMFs.

The scatter is of critical importance at these masses: we consider the BHMF derived from $M_{\text{BH}} - \sigma$ if we change the estimated intrinsic scatter by just 25% (i.e. within the range 0.27–0.36 dex), all within the range allowed by the present observations (Tremaine et al. 2002), and find that this relatively small difference in the intrinsic scatter estimate makes a larger difference at high M_{BH} than the choice of correlation ($M_{\text{BH}} - \sigma$, $M_{\text{BH}} - M_*$, or BHFP) adopted. This reinforces the point emphasized by Yu & Tremaine (2002); Yu & Lu (2004); Tundo et al. (2006) that the estimated intrinsic scatter can dominate the demographics of high-mass BHs – accounting for this, the BHFP does not substantially change these estimates.

6. THE PHYSICAL ORIGIN OF THE FUNDAMENTAL PLANE

If BH growth terminates because of self-regulation, the fundamental requirement is that sufficient energy be released to unbind the surrounding galactic gas. Given a radiative efficiency ϵ_r and feedback coupling efficiency η , the energy coupled to the IGM from accretion onto the BH over its lifetime is simply

$$E_{\text{BH}} = \eta \epsilon_r M_{\text{BH}} c^2 \quad (8)$$

and the binding energy of the gas in the center of the galaxy is

$$E_{\text{gas}} = \tilde{\phi} f_{\text{gas}} M_* \sigma^2, \quad (9)$$

where $\tilde{\phi}$ is a constant that depends on the shape of the bulge profile ($\tilde{\phi} = 10.1$ for a Hernquist (1990) profile). In detail, the energy in Equation 8 is proportional to the accreted (as opposed to the total) BH mass, and the binding energy of the bulge changes as a function of time during the merger. However, this simple estimate is actually a reasonable approximation to what occurs in the simulations, for two reasons.

First, as is also demanded by numerous empirical constraints (e.g., Soltan 1982; Hopkins et al. 2007f), the majority ($\gtrsim 70$ –80%) of the BH growth occurs in the observed “quasar” phase, which is constrained to be both short-lived (e.g. Martini 2004) and near-Eddington (e.g. Kollmeier et al. 2006), as occurs in the final growth phase near the end of the merger. Therefore, most of the final M_{BH} is accreted in the final e -folding of BH growth, over a Salpeter time $t_S \sim 4.2 \times 10^7$ yr. This is small compared to the cooling time of the galactic gas at $\sim R_e$, so the approximation that the energy released $\sim M_{\text{BH}}$ is reasonable. Second, by the time of the quasar phase, the merging galaxies have coalesced, and

the bulge is largely formed and in place, so the BH growth occurs in the relatively fixed potential of the remnant.

Equating the energy needed to unbind the surrounding gas and terminate accretion yields the expected scaling

$$M_{\text{BH}} \approx 10^8 M_{\odot} \frac{0.005}{\eta \epsilon_r / f'_{\text{gas}}} \left(\frac{M_*}{10^{11} M_{\odot}} \right) \left(\frac{\sigma}{200 \text{ km s}^{-1}} \right)^2, \quad (10)$$

where we adopt a Hernquist (1990) profile and a typical $\epsilon_r = 0.1$, $\eta \sim 0.05$ (similar to the values adopted in our simulations), which roughly reproduces the observed $M_{\text{BH}} - M_*$ normalization. Note that, in detail, the BH feedback need not be radiative – kinetic wind or jet feedback could inject comparable energy (e.g., Maraschi 2004; Tavecchio et al. 2004; Merloni et al. 2005), with some efficiency $E = \tilde{\eta} M_{\text{BH}} c^2$. This yields an identical Equation (10), as $\tilde{\eta}$ is functionally equivalent to the previous $\eta \epsilon_r$ – it does not matter in this derivation whether the net feedback efficiency ($\eta \epsilon_r$) represents a radiative or kinetic mode (or some sum of the two), or exactly what fraction of the final BH mass is accreted in a given growth phase, as the coupling efficiency simply serves to set the normalization of the M_{BH} -host correlations. It should also be noted that f'_{gas} changes by a large amount during the evolution of typical galaxies or (especially) mergers – the value relevant for Equation (10) is some effective value in the central regions near the BH during the final e -folding(s) of growth (hence the notation f'_{gas}), which does *not* necessarily trace the global or pre-active phase gas fraction of the system (see § 7).

We therefore naively expect that the BH mass should scale with $M_* \sigma^2$. In Figure 10, we examine the residuals of the best-fit correlation between M_{BH} and this binding energy $M_* \sigma^2$, in the manner of Figure 3. In this space, there does not appear to be any strong $\gtrsim 2\sigma$ evidence for a correlation of the residuals in $M_{\text{BH}}(M_* \sigma^2)$ with those of M_* , σ , or R_e . It seems that the correlation between BH mass and bulge binding energy is in some sense more basic than the correlation between BH mass and e.g. M_* or σ . However, when we fit M_{BH} to a function of $M_* \sigma^2$, we do *not* recover Equation (10) – in fact, a linear proportionality between M_{BH} and $M_* \sigma^2$ is ruled out at $\sim 5\sigma$ in the observations (and $> 10\sigma$ in our simulations). Instead, BH mass follows a “tilted” relation of the form

$$M_{\text{BH}} \propto (M_* \sigma^2)^{\alpha} \quad (11)$$

with $\alpha \approx 0.71$. Furthermore, this relation is not exactly the same as the BHFP we recover from the observations, which is closer to $M_{\text{BH}} \propto M_*^{0.5} \sigma^2$.

If we revisit our argument, we note that we have naively assumed that the accretion energy from the BH is coupled in an (effectively) infinitely short period of time and unbinds the surrounding gas. More properly, what occurs in our simulations is a pressure-driven outflow from the central regions (e.g., Hopkins et al. 2006b; Hopkins & Hernquist 2006). This implies that the necessary condition for self-regulation is the injection of sufficient momentum (at a rate $\dot{p} \propto L/c$; see e.g. Murray et al. 2005) to drive a galactic outflow (total $\dot{p} \propto M_* \sigma$) within the dynamical time near the radius of influence of the BH ($R_{\text{BH}} \equiv GM_{\text{BH}}/\sigma^2$),

$$t_{\text{dyn}}(R_{\text{BH}}) \approx \frac{R_{\text{BH}}}{\sigma} = \frac{GM_{\text{BH}}}{\sigma^3}. \quad (12)$$

When the rate is below this threshold, it can drive material from the central regions where it is initially bound or infalling onto the BH, but the momentum coupled is insufficient to

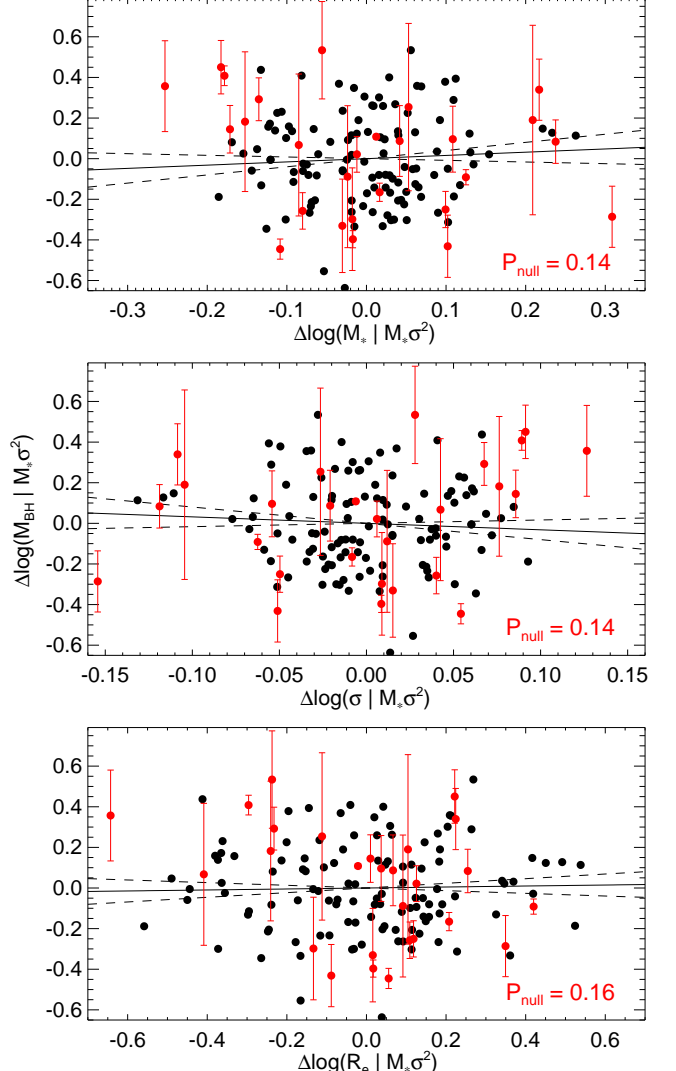


FIG. 10.— As Figure 3, but comparing the residuals in BH mass and host properties M_* , σ , and R_e at fixed spheroid binding energy $M_* \sigma^2$. There is no significant evidence in the simulations or observations for a residual correlation in this space. This is because the fundamental plane in BH mass can be (approximately) represented as a “tilted” correlation between BH mass and bulge binding energy, $M_{\text{BH}} \propto (M_* \sigma^2)^{0.71}$.

entrain the larger-scale material and the outflow fails to halt accretion (typical of the early-stage weak winds seen in our simulations in earlier merger stages; see Figure 1 in Cox et al. 2006a). This condition gives us the requirement

$$\dot{p} \Delta t \propto M_{\text{BH}}^2 / \sigma^3 \propto M_* \sigma, \quad (13)$$

or

$$M_{\text{BH}} \propto M_*^{1/2} \sigma^2, \quad (14)$$

similar to the observed BHFP.

Ultimately, the qualitative conclusions of these derivations are similar. Empirical constraints (e.g., Soltan 1982) demand that most BH mass is accumulated in high Eddington ratio quasar phases – so the details of accretion at lower Eddington ratios (whether set by e.g. the Bondi-Hoyle rate or other accretion mechanisms) are not important. This also implies that the BH mass is accumulated in a short period of time $\sim 10^7 - 10^8$ years, such that whether growth is driven at the end of galaxy mergers, or in secular disk or bar instabilities, the environment

(background potential) local to the BH is relatively fixed. The BH then self-regulates when it is sufficiently massive that its feedback energy can unbind infalling gas and halt accretion. Effects which deepen the local potential at the galactic center and increase the binding energy of gas near the BH will prevent gas from being unbound until the BH has grown more massive than it would otherwise. For example, as we show in detail in § 7, if spheroid progenitors are more gas-rich, there is more gas which can cool and form stars on small scales in the center of the spheroid, deepening the potential well there (i.e. yielding a more concentrated remnant with smaller R_e and larger σ , while having little effect on the total stellar mass). This requires that any BH grow larger in order to unbind nearby gas and halt accretion, in a manner similar to the scaling of Equation (14).

We might also ask how sensitively this BHFP scaling or “tilt” is related to dissipational processes, as Robertson et al. (2006b) demonstrate that the origin of the spheroid FP tilt lies essentially in the scale-dependence of dissipational processes such as gas cooling and star formation. From the derivation above, we would expect that although the processes from Robertson et al. (2006b) might affect the structure of the merger remnants themselves, they should not change how, fundamentally, the central BH self-regulates. Unfortunately, BH accretion is, itself, naturally a dissipational process, and therefore we cannot simply test this theory in our case by running simulations where gas dissipation is turned off.

However, Robertson et al. (2006b) further show that it actually requires substantial initial gas fractions for these dissipational effects to act – in mergers with very low initial gas fractions ($\lesssim 20\%$) no “tilt” (in the spheroid FP) is induced, consistent with requirements from the observed phase space densities of ellipticals (e.g., Hernquist et al. 1993). We therefore briefly consider just a set of simulations with initial $f_{\text{gas}} = 0.05$. This is sufficiently low that the remnants act dissipationlessly, and lie on the virial relation as opposed to the spheroid FP (see Figure 10 of Robertson et al. (2006b)), but sufficiently large that we do not need to worry about artificially “strangling” the BH by giving it insufficient gas to accrete (given typical $M_{\text{BH}} \approx 0.001 M_*$, the BH need only have access to $\sim 2\%$ of this gas to grow normally).

We find that these merger remnants obey a similar BHFP relation to their high- f_{gas} counterparts, implying that so long as feedback-driven self-regulation (as opposed to e.g. gas starvation) determines the final BH mass, these scalings are robust. However, the significance of the preference for e.g. a BHFP relation as opposed to a simpler $M_{\text{BH}} \propto M_*$ or $M_{\text{BH}} \propto \sigma^4$ relation is greatly reduced. This is because, without significant effects of dissipation to change the central phase-space structure and potential depth of the remnant, the velocity dispersion σ and effective radius R_e are simply set by the violent relaxation of the scattered stellar disks. The general scalings of the BHFP are not, then, unique to gas-rich progenitors, but their significance and the importance of accounting for the observed dependencies are so.

Indeed, regardless of prescriptions for BH accretion, feedback, and star formation, the above derivations (and qualitative dependence on galaxy properties) depend on only three relatively robust assumptions – that BH growth is dominated by bright, high-Eddington ratio phases, that feedback from accretion affects the gas on small scales around the BH (sensitive to the central potential of the galaxy), and that some sort of heating, momentum coupling, or

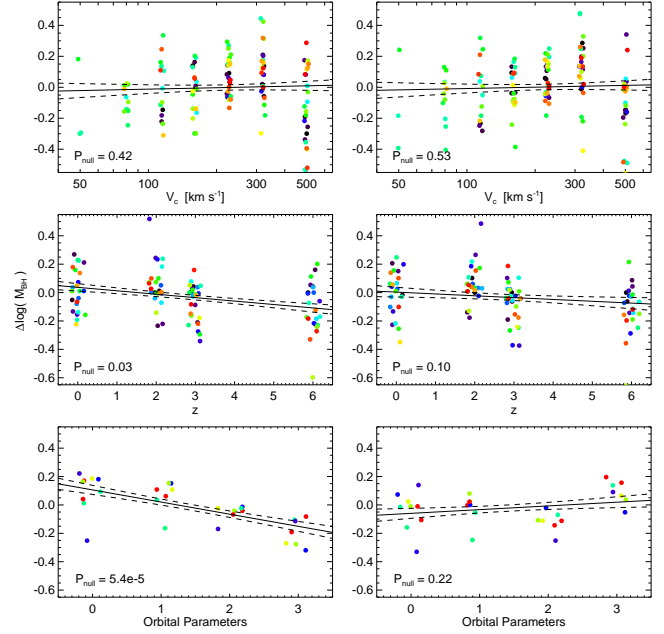


FIG. 11.— Residuals of the $M_{\text{BH}} - M_*$ (left) and BHFP (right) relations as a function of various initial conditions or theoretical quantities. V_c is the halo virial velocity, z is the redshift to which the progenitor disks are initialized (i.e. their concentrations and scale lengths are rescaled by a small amount to match disks at these redshifts), and the orbital parameters shown span a small set ranked from those that yield the least (0) to most (3) rotation in the merger remnants (average $(V_c/\sigma)^*$ = 0.06, 0.25, 0.41, 1.03, respectively; for details, see Cox et al. 2006b). By changing e.g. the circular velocities, initial disk formation redshifts, or orbital parameters of simulated mergers, we can drive changes in the $M_{\text{BH}} - M_*$ relation. However, these can all be understood in terms of how they change the galaxy structure – i.e. they drive changes in σ at fixed M_* , while preserving the BHFP relation. Higher angular momentum mergers also produce more disk-like remnants – but when we are careful to exclude the contribution from rotation to the velocity dispersion σ , the objects lie on the expected BHFP.

effective pressure eventually halts accretion. This does place some constraints on scenarios for BH growth, however. In models where, for example, the BH accretion rate is a pure function of the galactic star formation rate (see e.g., Kawakatu et al. 2006; Monaco & Fontanot 2005; Granato et al. 2004; Cattaneo et al. 2005, although in some of these cases the Eddington limit is still preserved as an upper limit), it is difficult to explain how the BH mass would be sensitive to the central potential in the manner of the observed BHFP, and not simply trace the galaxy stellar mass (i.e. a yield pure $M_{\text{BH}} - M_*$ relation, which the observations disfavor at $\sim 3\sigma$).

7. DRIVING SYSTEMS ALONG THE FUNDAMENTAL PLANE

We have thus far considered systems in terms of the observable properties of the remnants, specifically quantities like M_* , σ , and R_e . We now turn to the “theorist’s question” – namely, how are the positions of systems on the $M_{\text{BH}} - M_*$, $M_{\text{BH}} - \sigma$, and BHFP relations affected by theoretical quantities or initial conditions?

Figure 11 considers the residuals in the $M_{\text{BH}} - M_*$ and BHFP relation for merger remnants with different virial velocities, redshifts, and orbital parameters. Note that “redshift” in this context simply refers to the characteristics of the progenitor disks (which are initialized to resemble disks at low redshifts $z \sim 0$, or higher, $z = 2, 3, 6$). We select each set of simulations in which all parameters are identical except that plotted in the figure, then consider the residual with respect to

the mean relation for just those simulations (each set of points of different color plotted in the figure represents one such set of simulations).

In terms of M_{BH}/M_* , there are weak ($\sim 0.2 - 0.3$ dex over the maximal range spanned by the simulations) trends towards lower M_{BH}/M_* for higher redshift and larger angular momentum mergers, but the systems lie on the same BHFP regardless of V_{vir} , z , orbital parameters, or any other initial quantities we vary. The trends in M_{BH}/M_* simply reflect changes in the structural properties of the remnants – for example, particular orbital parameters produce smaller bulges and lower values of σ at fixed M_* . This is expected – because most of the BH growth occurs over a short period of time at the end of a merger or other phase of activity (the last 1-2 e -folding times) during which the environment is relatively dynamically settled, changing initial conditions should only affect M_{BH} indirectly by altering the central structure of the remnant. The lack of a strong trend in V_{vir} simply reflects the fact that the central regions which set the potential depth of relevance for determining M_{BH} are very much baryon-dominated. This is not to say that M_{BH} does not scale with V_{vir} , in a mean sense, but simply that the dependence on V_{vir} is subsumed in the more direct dependence on M_* and σ , which themselves can depend on halo mass or V_{vir} .

For this reason, at fixed $M_*^{1/2} \sigma^2$, we expect BH mass to be independent of halo mass and redshift. Of course, M_* and σ will, in the mean, scale with M_{halo} , which could yield evolution in the $M_{\text{BH}} - M_{\text{halo}}$ relation. For a bulge-dominated system (i.e. ignoring the complication that the same mass halo could host a disk-dominated system with a much smaller BH), $M_* = f_*(\Omega_b/\Omega_m)M_{\text{halo}}$, where $f_*(M_{\text{halo}}, z)$ is the typical fraction of baryons incorporated into the galaxy. In the simulations, we find a rough correlation $\sigma \propto v_{\text{max}}$ (similarly, $v_c \propto v_{\text{max}}$ for our progenitor disks, although that is by construction), where v_{max} is the maximum halo circular velocity ($\propto V_{\text{vir}} c^{1/2}$, where $c(M_{\text{halo}}, z)$ is the halo concentration), modulo the effects of e.g. gas fraction and orbital parameters changing σ at fixed M_{halo} . Observationally, a similar mean correlation ($\sigma \approx 0.66 v_{\text{max}}$, nearly identical to the best-fit normalization in our simulations; e.g. Kronawitter et al. 2000; Gerhard et al. 2001) is found. Given $c \propto M_{\text{halo}}^{-0.13} (1+z)^{-1}$ (Bullock et al. 2001), this implies $M_{\text{BH}} \propto \alpha(z) f_*^{0.5} M_{\text{halo}}^{1.04}$, where $\alpha(z)$ represents the weak remaining redshift evolution term, $\alpha \equiv (\Omega_m \Delta_c(z)/\Omega_m(z) 18\pi^2)^{1/3}$, which changes by only $\sim 20\%$ from $z = 0 - 6$. We therefore expect that evolution in the $M_{\text{BH}} - M_{\text{halo}}$ relation will be dominated by the effects of evolution in typical gas fractions and remnant structural properties on σ (changing σ at fixed M_{halo} in a systematic sense) as well as cosmological evolution in typical baryon incorporation fractions f_* and/or bulge-to-disk ratios in galaxies hosted by halos of a given mass. To the extent that such effects occur, they of course should be also traced in some mean evolution in e.g. the $\sigma - v_{\text{max}}$ relations.

We have also studied a large subset of simulations of different masses and gas fractions with a variety of prescriptions for feedback and winds from star formation. These results will be discussed in detail in Cox et al. 2007 (in preparation), but we briefly summarize their relevant conclusions. The inclusion of massive stellar winds (with high mass loading efficiencies $\eta_w \gtrsim 1$, where $\dot{M}_{\text{wind}} = \eta_w \dot{M}_*$) can affect the structure of merger remnants, although not necessarily in a monotonic or easily predictable fashion. For example, strong winds can remove gas from the central regions of the galaxy and

yield a lower effective gas fraction f_{gas} , but they can also cycle such gas at earlier stages, preventing it from immediately being turned into stars before the final merger, and actually raising the effective f_{gas} at the final coalescence. In any case, the effects are usually small (especially in the most massive galaxies of interest here) or comparable to those owing to the choice of orbital parameters.

More important, regardless of the stellar feedback efficiency, star formation alone cannot prevent gas from accreting onto the central BH (especially given that only $\sim 0.1\%$ of the galaxy mass in gas needs to reach the BH to affect the M_{BH} -host correlations), and in fact strong stellar winds can (either by cycling gas as above, or by shocking and increasing the supply of low angular momentum material) greatly increase the fuel supply for accretion at the galactic center. The correlation between BH mass and host properties is therefore, regardless of the prescription for stellar feedback, still set by the local self-regulation of the BH, and obeys (in all our simulations) an identical BHFP relation. Stellar winds can, in principle, influence the final BH mass, but only indirectly by affecting the structure of the remnant, in the same manner as changing progenitor structural properties, orbital parameters, and gas fractions.

Figure 12 considers the trend in M_{BH}/M_* as a function of the initial gas fraction of our simulations. In contrast to trends with V_{vir} , orbital parameters, or the evolution of disk structural parameters with redshift, the dependence of M_{BH}/M_* on f_{gas} is quite strong, varying by nearly an order of magnitude from low ($f_{\text{gas}} \lesssim 0.2$) to high ($f_{\text{gas}} \gtrsim 0.8$) initial gas fractions. We consider this in detail by examining a small case study set of simulations. We construct a fiducial set of simulations of Milky-Way like initial disks ($V_{\text{vir}} = 160 \text{ km s}^{-1}$), and collide them in otherwise identical mergers except for varying the initial disk gas fractions with values $f_{\text{gas}} = 0.05, 0.2, 0.4, 0.6, 0.8, 1.0$. We construct three such suites, each with a different orbit (roughly bracketing the extremes of possible merger configurations). Figure 12 also shows the trend of M_{BH}/M_* in these simulations – it is clear that, all else being equal, larger values of f_{gas} drive the systems to larger M_{BH}/M_* .

However, the trend here does *not* resemble the simple $M_{\text{BH}} \propto f_{\text{gas}}$ scaling that we naively predicted in Equation (10) by demanding that the BH be able to unbind the entire initial gas content of the galaxy. In fact, Figure 13 shows the correlation between M_{BH} and $M_* \sigma^2$ for simulations of different gas fractions, and there is no systematic trend with f_{gas} . Likewise, the remnants lie on the BHFP regardless of their gas fractions – i.e. the change in M_{BH}/M_* can be entirely accounted for by the change in σ at fixed M_* . This should, perhaps, not be surprising – our earlier derivation neglected the fact that, by the quasar phase and epoch of final BH growth, the large majority ($\gtrsim 80 - 90\%$) of f_{gas} has already been turned into stars or ejected by stellar winds. The trend in M_{BH}/M_* with f_{gas} must therefore be primarily driven by how f_{gas} changes the structural properties of the remnant, a more subtle effect than the naive “amount of material to be unbound” expectation.

In order to understand this strong dependence of M_{BH}/M_* on f_{gas} , we consider the structural properties of the merger remnants in our case study in Figure 14. On inspection, it is clear that the trend in M_{BH}/M_* is one of increasing M_{BH} at fixed M_* , as M_* is nearly constant with f_{gas} (there is a weak trend, as not all of f_{gas} is converted to stars, but this changes M_* by < 0.1 dex from $f_{\text{gas}} = 0$ to $f_{\text{gas}} = 1$). However, there is a

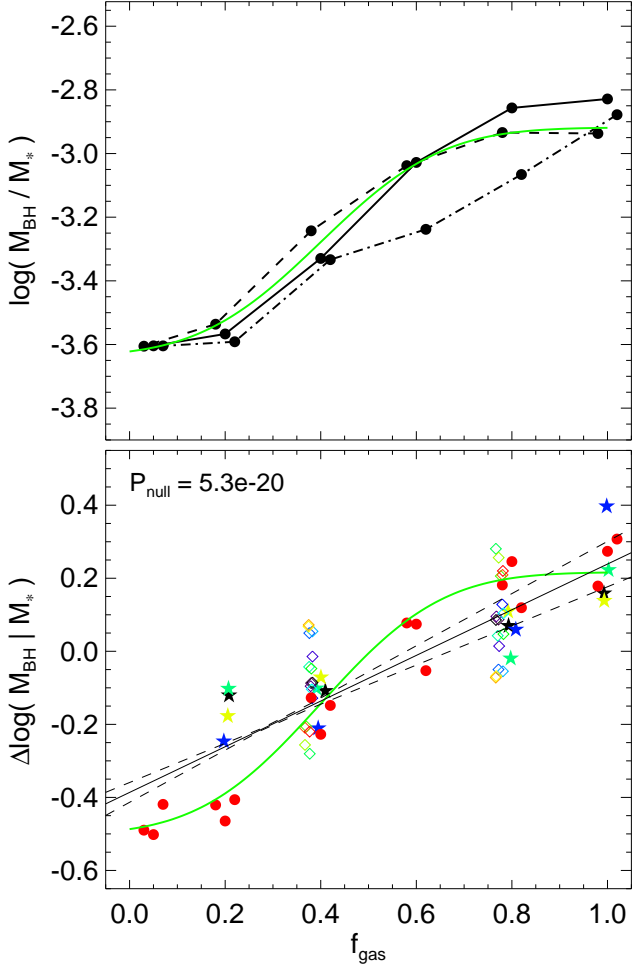


FIG. 12.— Trend in M_{BH}/M_* as a function of simulation initial disk gas fraction. Upper panel plots M_{BH}/M_* for three suites of simulations (solid, dashed, and dot-dashed lines). Each of the three is a set of otherwise identical mergers of Milky Way-like systems, varying only the gas fraction with values $f_{\text{gas}} = 0.05, 0.2, 0.4, 0.6, 0.8, 1.0$. The three suites consider three different orbital configurations for the merger. Lower panel considers these residuals and those from our other simulations versus f_{gas} as in Figure 11. Black line is a log-linear fit (dashed show $\pm 1\sigma$), green line the more accurate fit $\log(M_{\text{BH}}/M_*) = -3.27 + 0.36 \text{erf}[(f_{\text{gas}} - 0.4)/0.28]$. High- f_{gas} mergers produce much larger BHs than low- f_{gas} systems.

strong trend in R_e and σ with f_{gas} , as increasing the amount of dissipation (through f_{gas}) yields more concentrated remnants.

We can understand this behavior with a simple toy model. Assume that the stars formed in the disk(s) before and during the merger (i.e. those that will act dissipationlessly) are scattered into a typical bulge with a Hernquist (1990) profile with scale length $R_e(f_{\text{gas}} = 0)$, independent of the central gas content, and that a fraction μ of the initial gas mass ($M_{\text{gas}} = f_{\text{gas}} M_{\text{gal}}$) survives to the late stages of the merger and, via dissipation, falls to the center of the galactic potential. There, it will form a highly concentrated central stellar component (scale length $\ll R_e(f_{\text{gas}} = 0)$; for simplicity we take it to be effectively a point concentration). The total enclosed mass as a function of radius is then

$$M_{\text{gal}}(< r) = M_{\text{gal}} \left[\mu f_{\text{gas}} + \frac{(1 - \mu f_{\text{gas}}) r^2}{(r + R_e[f_{\text{gas}} = 0])^2} \right]. \quad (15)$$

This yields a half-mass effective radius R_e of

$$\frac{R_e}{R_e(f_{\text{gas}} = 0)} = \frac{x}{(\sqrt{2} + 1)(1 - x)} \quad (16)$$

$$x = \left(\frac{1/2 - \mu f_{\text{gas}}}{1 - \mu f_{\text{gas}}} \right)^{1/2}.$$

Figure 14 compares this simple expectation for R_e and $\sigma^2 \propto M_*/R_e$ with that from the simulations as a function of f_{gas} – for a representative $\mu = 0.5$, our toy model describes the simulations quite well (until $f_{\text{gas}} \rightarrow 1$, where our assumption that the inner stellar component is infinitely concentrated breaks down; this “saturation” in σ reflects the fact that even extremely gas-rich systems will still turn much of that gas into stars that scatter into some large orbits, and may be important for e.g. the steep observed cutoff in the observed σ distribution). Note that this scaling is not very sensitive to our assumption about the exact profile shape – assuming the bulge follows an exact $r^{1/4}$ law or adopting a different inner power-law slope changes the predicted scaling by only $\sim 10 - 20\%$. Given this change in R_e at fixed M_* owing to increasing f_{gas} , the fundamental plane implies that M_{BH} should increase, roughly as $\sim R_e^{-1}$. Figure 15 plots the dependence of M_{BH}/M_* on f_{gas} , compared with the expectation from this simple model. From the agreement here, and the fact that Figure 14 finds no change in the BHFP with f_{gas} , we conclude that more gas-rich mergers drive evolution in M_{BH} by producing more concentrated remnants with smaller R_e and larger σ at fixed M_* , and therefore larger $M_* \sigma^2$.

There is one important caveat to our discussion of disk gas fractions f_{gas} . Lacking a full cosmological simulation in which to determine how gas continuously accretes onto the disks, we have simply referred to f_{gas} as the initial gas fraction in our simulations. Of course, during a simulation, f_{gas} will decrease as gas is turned into stars, so that the actual gas fractions by the time the systems merge may be substantially lower than the numbers we quote. In Figure 15, we reproduce our plot from Figure 12 of the residuals in M_{BH}/M_* as a function of the initial gas fraction of the simulations. However, we also return to the simulations and measure the gas fraction for each at a set of uniform times $\Delta t = 1.0, 0.5$, and 0.2 Gyr before the final merger (defined for convenience as the coalescence of the two BHs). As the simulations approach the final merger event, it is clear that the trend of residuals with f_{gas} is qualitatively unchanged – however, the absolute values of f_{gas} systematically decrease. By $\Delta t = 0.2$ Gyr, the gas fractions are systematically lower by a factor $\sim 2 - 3$. Therefore, the exact values of f_{gas} which we quote should not be taken too literally – if gas is accreted in the real universe such that f_{gas} changes less rapidly in earlier stages of a merger, then the initial gas fraction need only be as large as $f_{\text{gas}} \sim 0.3$ to be equivalent to our most extreme $f_{\text{gas}} = 1$ cases (with our more typical $f_{\text{gas}} = 0.4 - 0.5$ cases corresponding to rather moderate pre-merger or $\Delta t = 0.2$ Gyr gas fractions of ~ 0.2).

8. IMPLICATIONS FOR THE REDSHIFT EVOLUTION IN BH-HOST RELATIONS

8.1. Empirical Predictions

Given that the BHFP appears to be robust against all varied quantities in our simulations, we expect that it should be preserved at all redshifts. However, this implies that, at fixed M_* , evolution with redshift in the typical velocity dispersions and/or effective radii of spheroids will also manifest as evolu-

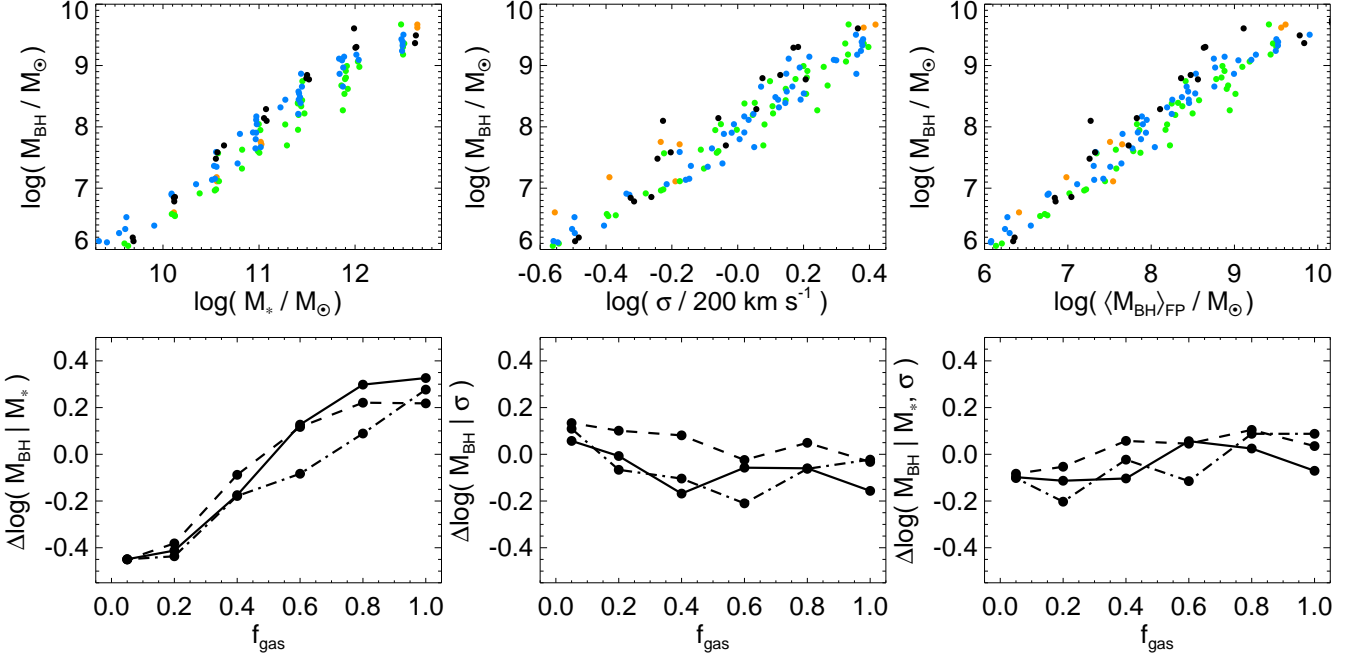


FIG. 13.— *Left:* Correlation of M_{BH} with M_* in simulations with different gas fractions $f_{\text{gas}} = 0.2, 0.4, 0.8, 1.0$ (orange, green, blue, and black, respectively; *upper*), and residuals of $M_{\text{BH}} - M_*$ as a function of f_{gas} for our case study simulations from Figure 12 (*lower*). *Center:* Same, but for the $M_{\text{BH}} - \sigma$ correlation. *Right:* Same, but for the BHFP relation. Varying f_{gas} does not move the remnants off the BHFP relation, but does systematically shift them with respect to M_* and σ . The trend of M_{BH}/M_* with f_{gas} in Figure 12 must therefore fundamentally relate to how f_{gas} modifies structural properties like σ (preserving the BHFP), not to the naive expectation that larger f_{gas} translates to “more material to be unbound.”

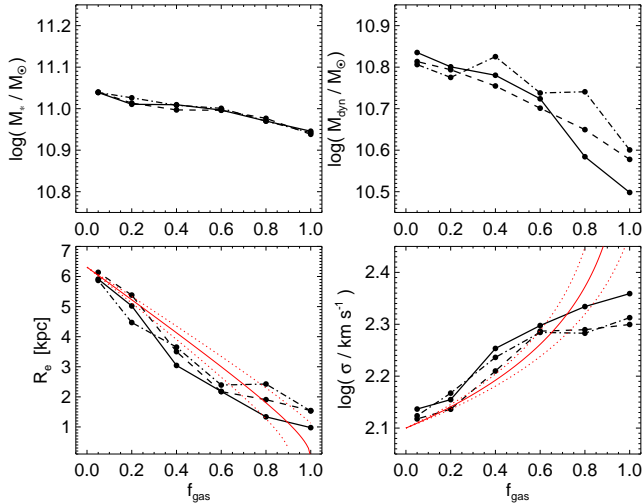


FIG. 14.— The structural properties of the merger remnants from our set of gas fraction case studies from Figure 12. Changing f_{gas} has almost no effect on M_* , but by increasing the amount of dissipation and fraction of stellar material formed in the final, central starburst, increasing f_{gas} produces more concentrated remnants with smaller effective radii R_e and larger central velocity dispersions σ . Red lines show the expectation of a toy model in which a fraction ~ 0.5 (solid; ± 0.05 , dashed) of the gas participates in a central starburst (Equation 16).

tion in the typical M_{BH}/M_* relation.

It is observed empirically (Trujillo et al. 2006) and expected theoretically (Khochfar & Silk 2006) that high-redshift spheroids will be more compact at a given stellar mass M_* than their low-redshift analogues. Specifically, Trujillo et al. (2006) compile a number of measurements of the evolution, relative to $z = 0$, of the effective radii of spheroids (defined as systems with Sersic indices $n_s > 2.5$) at fixed stellar mass $M_* > 3 \times 10^{10} M_\odot$ and $> 6 \times 10^{10} M_\odot$,

corresponding to typical L_* galaxies at most redshifts. If the BHFP is preserved, this necessarily implies evolution in the $M_{\text{BH}} - M_*$ relation, of the form $M_{\text{BH}}/M_* \propto R_e(M_*)^{-1}$ (see Table 1 for exact values).

Figure 16 plots this expected evolution in M_{BH}/M_* from the Trujillo et al. (2006) measurements, normalized to the value observed at the same stellar mass by Häring & Rix (2004) at $z \approx 0$. For comparison, we plot the estimated evolution in M_{BH}/M_* from Peng et al. (2006) (specifically, we adopt their early-type template to convert their measured luminosities to stellar masses), and limits on this evolution from Hopkins et al. (2006d), normalized to the same local value.

We can also attempt to empirically infer the evolution in M_{BH}/M_* by considering the clustering of quasars as a function of redshift. Essentially, this expands on the measurement in Adelberger & Steidel (2005). A more detailed discussion of this (and the samples we consider) is given in Hopkins et al. (2007e) and Fine et al. (2006), but we briefly review it here.

We consider a quasar sample (typically observed near $\sim L_*$ in the quasar luminosity function) for which BH masses or typical Eddington ratios have been directly measured (for 2dF quasars, we directly adopt the observed BH mass distributions from Fine et al. (2006), otherwise we use those determined as a function of quasar luminosity and redshift in Kollmeier et al. (2006)). We then use the observed clustering properties of that sample to infer a characteristic host halo mass – in other words, match the observed large-scale bias of the quasar population to the average (number-density weighted) large-scale bias for halos in some mass range (at the same redshift). We calculate the expected large scale bias of halos as a function of mass following Mo & White (1996) with the improved fitting formulae from Sheth et al. (2001). If we assume the ratio of galaxy to halo mass for $\sim L_*$ galaxies does not evolve much with redshift (which appears to be observationally confirmed to at least $z \sim 1$; see e.g. Heymans et al. 2006; Conroy et al.

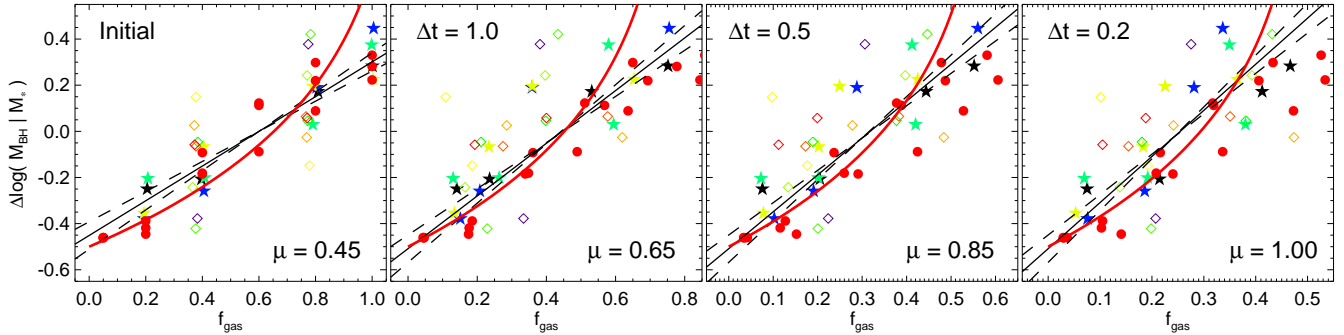


FIG. 15.— Dependence of M_{BH}/M_* on f_{gas} , as in Figure 12. Panels plot this as a function of f_{gas} measured at the initial time in each simulation (left) and at times $\Delta t = 1.0$, 0.5 , and 0.2 Gyr before the final merger and quasar phase. Black lines in each plot the best-fit trend (solid; with $\pm 1\sigma$ range in dashed lines), and red lines plot the expectation from our simple model (Equation 16), assuming that the BHFP is always preserved and that a fraction μ of the gas mass measured at each time will participate in the final, central starburst (μ is smaller at early times because much of this gas will form stars in the two disks well before they merge). Regardless of when f_{gas} is defined, the trend is similar, and evolution in M_{BH}/M_* is driven by preserving the BHFP and increasing σ at fixed M_* in the same manner.

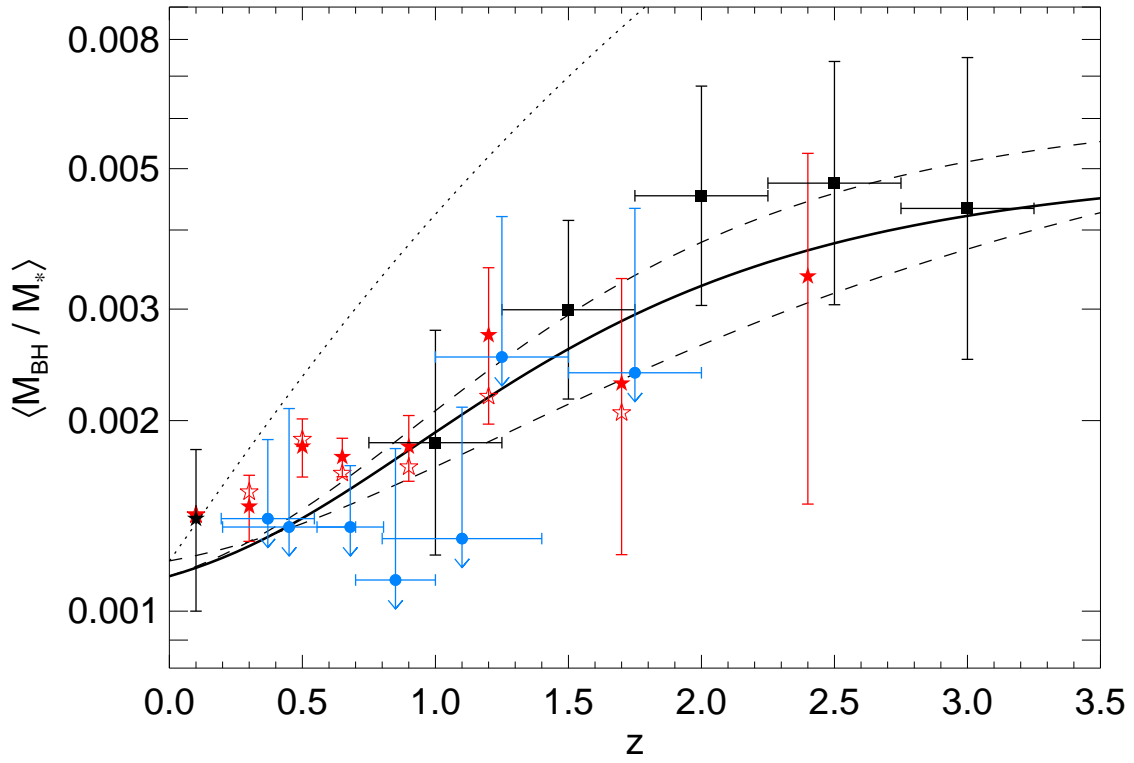


FIG. 16.— Evolution in M_{BH}/M_* as a function of redshift. Red stars plot the evolution expected at fixed M_* (filled $\sim 6 \times 10^{10} M_\odot$; open $\sim 3 \times 10^{10} M_\odot$) given the observed evolution in the effective radii $R_e(M_*)$ for systems of this stellar mass from Trujillo et al. (2006) and our fundamental plane relations (Table 1). Other points compare observational estimates of this evolution: black squares are direct measurements of high-redshift BH masses and host luminosities (Peng et al. 2006), blue circles are upper limit estimates from Hopkins et al. (2006d) based on observed spheroid and BH mass functions. All points are normalized to the same local value (black star) from Härting & Rix (2004). Solid and dashed lines show the predicted evolution from an *a priori* model in which the evolution in $R_e(M_*)$ (and, correspondingly, $M_{\text{BH}}(M_*)$) is driven by increasing disk gas fractions with redshift, given the best-fit scalings of $M_{\text{BH}}(f_{\text{gas}} | M_*)$ (solid; dashed show $\pm 1\sigma$). The BHFP predicts that as high-redshift spheroids are more compact, M_{BH}/M_* must rise, in good agreement with the observations; the trend is driven by more gas-rich progenitors in spheroid-producing mergers. To contrast, dotted line shows the expectation of the simplified (but common) semi-analytic assumption that $M_{\text{BH}} \propto \sigma^4 \propto V_c^4$ (assuming $M_*(M_{\text{vir}})$ does not change much with z for $\sim L_*$ galaxies).

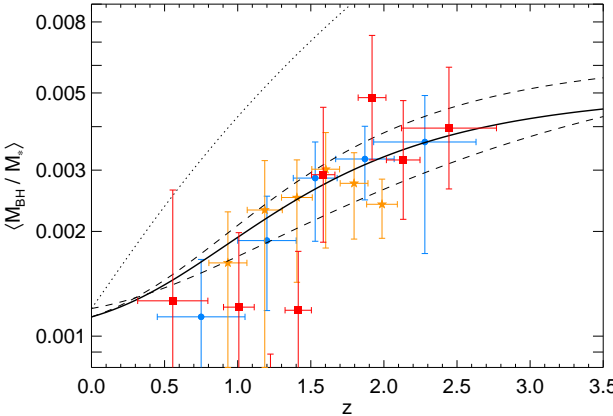


FIG. 17.— As Figure 16 (solid and dashed lines are our prediction and $\pm 1\sigma$ range, respectively; dotted line is an alternative $M_{\text{BH}} \propto V_c^4$ model), but the observationally estimated evolution of M_{BH}/M_* (points) is derived from measurements of quasar clustering as a function of redshift, following Fine et al. (2006). For quasars of a given (measured) BH mass, their clustering implies a characteristic host halo mass – if the ratio of that halo mass to stellar mass does not change with redshift, then the implied M_{BH}/M_* evolves as plotted (see Hopkins et al. (2007e) and Fine et al. (2006) for details). Measurements of quasar clustering are taken from Fine et al. (2006, red squares) and Porciani & Norberg (2006, orange stars) from the 2dF, and Myers et al. (2006, blue circles) from the SDSS.

2007; Zheng et al. 2007), then we have (implicitly) obtained the average host galaxy mass of these quasars, for which we know M_{BH} – i.e. an estimate of the mean $M_{\text{BH}}/M_*(z)$. Of course, the bias as a function of halo mass will depend on the cosmology adopted (specifically the value of σ_8); this and e.g. the BH mass measurements from quasar spectral energy distributions all introduce fairly large systematic uncertainties (at least factor ~ 2) in the absolute implied value of M_{BH}/M_* . However, to the extent that we are interested only in the *relative* evolution of this with redshift, these uncertainties are much smaller.

Compiling a number of measurements of quasar clustering as a function of redshift, the inferred evolution in M_{BH}/M_* is shown in Figure 17. This provides a completely independent measurement of M_{BH}/M_* from that of Peng et al. (2006), with entirely different systematics, but nevertheless is in reasonable agreement with their estimates, and with our simple expectation from the BHFP relation. Of course, the present observations are not sufficiently robust to distinguish between evolution by a factor of ~ 2 versus evolution by a factor of ~ 3 at high redshifts, but different probes seem to suggest a roughly comparable effect to that predicted.

8.2. A Dissipation-Driven Explanation

Given the BHFP, we have the empirical expectation that, at high redshift as spheroids become more concentrated, M_{BH} must be larger at fixed M_* . However, this does not explain what physically drives these trends. In § 7, we showed that increasing the gas fractions of merger progenitors has both of these effects: namely, that by increasing the amount of dissipation, more centrally concentrated remnants with smaller R_e , higher σ and larger M_{BH} at fixed M_* are produced. It is both expected and observed that high-redshift disks are characteristically more gas-rich, as star formation has simply had less time to operate – this provides a potential *a priori* physical motivation for the evolution we saw in § 8.1.

We therefore briefly examine how systematic evolution in the gas fractions of the progenitors of gas-rich, spheroid form-

ing mergers (i.e. disk galaxies) should affect the resulting M_{BH} -host galaxy correlations of the merger remnants (by, for example, increasing the amount of dissipation and therefore forming more compact, higher- σ remnants). To begin, we need to construct an estimate for how the gas fractions of typical disks evolve as a function of redshift. Fortunately, the structural properties (i.e. basic kinematics and the Tully-Fisher relation) of disks appear to evolve relatively weakly with redshift, so we can at least attempt to simply scale up from the properties of local disks (using e.g. their star-formation histories). Traditionally, the star formation histories of local disks are fitted to τ -models, of the form $\dot{M}_* \propto \exp[-(t - t_i)/\tau]$, where τ is some characteristic timescale and t_i is an initial time of formation. This is, of course, a non-unique parameterization of the star formation history, but nevertheless appears to be a reasonable description of average stellar populations (e.g., Noeske et al. 2007). For a system with stellar mass $M_*(z=0) = M_*(t=t_H)$ (t_H being the Hubble time at $z=0$), this implies a normalization

$$\dot{M}_*(t) = \frac{M_*(z=0)}{\tau} (1 - \exp[(t_i - t_H)/\tau])^{-1} \exp[(t_i - t)/\tau]. \quad (17)$$

It is also well-established that disks obey a Kennicutt-Schmidt star formation law (Kennicutt 1998) relating the surface density of star formation to the gas surface density as $\Sigma_{\text{SF}} \sim \Sigma_{\text{gas}}^{1.4}$. The total SFR $\dot{M}_* \propto \Sigma_{\text{SF}} R_d^2$, and $\Sigma_{\text{gas}} \propto M_{\text{gas}} R_d^{-2}$, where $M_{\text{gas}} = f_{\text{gas}} M_{\text{tot}} = f_{\text{gas}} (1 - f_{\text{gas}})^{-1} M_*$ and R_d is the disk scale length. Knowing, therefore, how the mean star formation rate in disks of a given mass evolves, and how this scales with the surface density of gas, we need only some estimate of their characteristic sizes (R_d) to infer the (mean) evolution in the total gas mass content. If the baryonic Tully-Fisher relation does not evolve with redshift, as suggested by observations (Conselice et al. 2005; Flores et al. 2006) – i.e. the kinematic structure of disks does not strongly evolve, then we have $M_{\text{tot}} \propto V_{\text{disk}}^4$ (Bell & de Jong 2001; McGaugh 2005, V_{disk} being the disk circular velocity = $\sqrt{GM_{\text{tot}}/R_d}$) and therefore $M_{\text{tot}} \propto R_d^2$. Combining the Tully-Fisher relation with the Schmidt-Kennicutt law then implies

$$\frac{\dot{M}_*(t)}{M_*(t)} \propto \frac{f_{\text{gas}}^{1.4}}{1 - f_{\text{gas}}}. \quad (18)$$

If we demand that the normalization of the Schmidt-Kennicutt law agree with the normalization from the fitted τ model, we then arrive at an equation for the implied evolution in f_{gas} ,

$$\frac{f_{\text{gas}}^{1.4}}{1 - f_{\text{gas}}} = \frac{f_0^{1.4}}{1 - f_0} \left(\frac{1 - \exp[(t_i - t_H)/\tau]}{1 - \exp[(t_i - t)/\tau]} \right) \exp[(t_H - t)/\tau], \quad (19)$$

where $f_0 = f_{\text{gas}}(z=0)$. Adopting the measured best-fit τ and $z=0$ gas fraction f_0 as a function of $z=0$ stellar mass M_* from Bell & de Jong (2000) and Kannappan (2004), respectively, we finally obtain an expected typical f_{gas} and SFR as a function of disk stellar mass at any cosmic time t .

Figure 18 compares the expected $f_{\text{gas}}(M_*(t))$ from this parameterization with that observed at a number of different redshifts. We also compare this estimate to another, even simpler parameterization we could adopt: assuming an isolated disk obeying a τ -model, with $f_{\text{gas}} = 1$ at $t = 0$ and $f_{\text{gas}} \approx 0.1$ (appropriate for a Milky Way-like $\sim L_*$ disk today) at $z = 0$. This implies an exponential growth of f_{gas} with lookback time, with e -folding time ~ 6 Gyr. The results are similar,

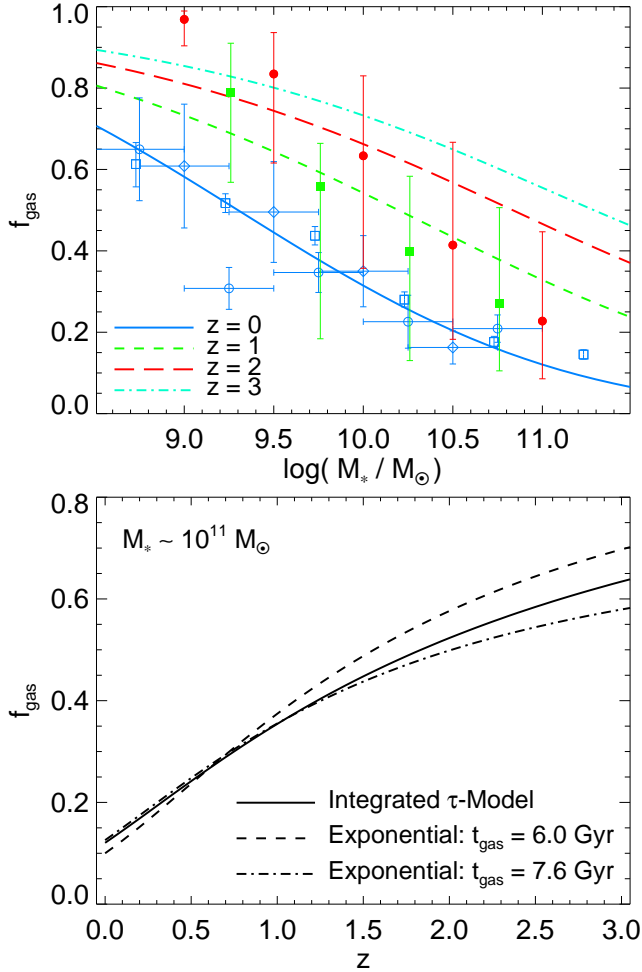


FIG. 18.— *Upper*: Comparing the predicted evolution in characteristic disk gas fractions (as a function of stellar mass) from our simple toy model (in which we integrate backwards in time the best-fit τ -model star formation histories of local disks) with that observed. We compare the expected mean $f_{\text{gas}}(M_*)$ with estimates at $z = 0$ (blue points; Bell & de Jong 2001; Kannappan 2004; McGaugh 2005, as diamonds, squares, &, circles respectively), $z \sim 1$ (green squares; estimated from H α luminosities Shapley et al. 2005), and $z \sim 2$ (red circles Erb et al. 2006). *Lower*: Evolution in f_{gas} from our simple empirical model for a constant $M_* = 10^{11} M_\odot$, compared to a simple exponential history with e -folding time t_{gas} (as labeled).

and appear to describe the observed f_{gas} evolution reasonably well. We have also checked that the expectation from Equation (18) is consistent with observed specific star formation rates as a function of M_* from $z = 0 - 3$ (see, e.g. Bauer et al. 2005; Feulner et al. 2005; Papovich et al. 2006), and find good agreement even up to $z \sim 3$ (which should not be surprising, as this essentially just says that the τ model is indeed a reasonable description of the mean star formation history).

Given this evolution in f_{gas} , we are now in a position to estimate how this should change the effective radii and velocity dispersions of merger remnants, and (given the BHFP) the average value of M_{BH} at fixed stellar mass M_* . Figure 19 shows the evolution of the $M_* - \sigma$ and $R_e - M_*$ relations with f_{gas} , from our simulations, where the behavior is similar to that we discussed in § 7. Combining the trend in $R_e(M_*)$ as a function of f_{gas} from our simulations, and the trend in $f_{\text{gas}}(z)$ above, we also then predict how $R_e(z)$ should evolve, at fixed M_* . Comparing this to the results from Trujillo et al. (2006) shows excellent agreement given our simple estimate of $f_{\text{gas}}(z)$.

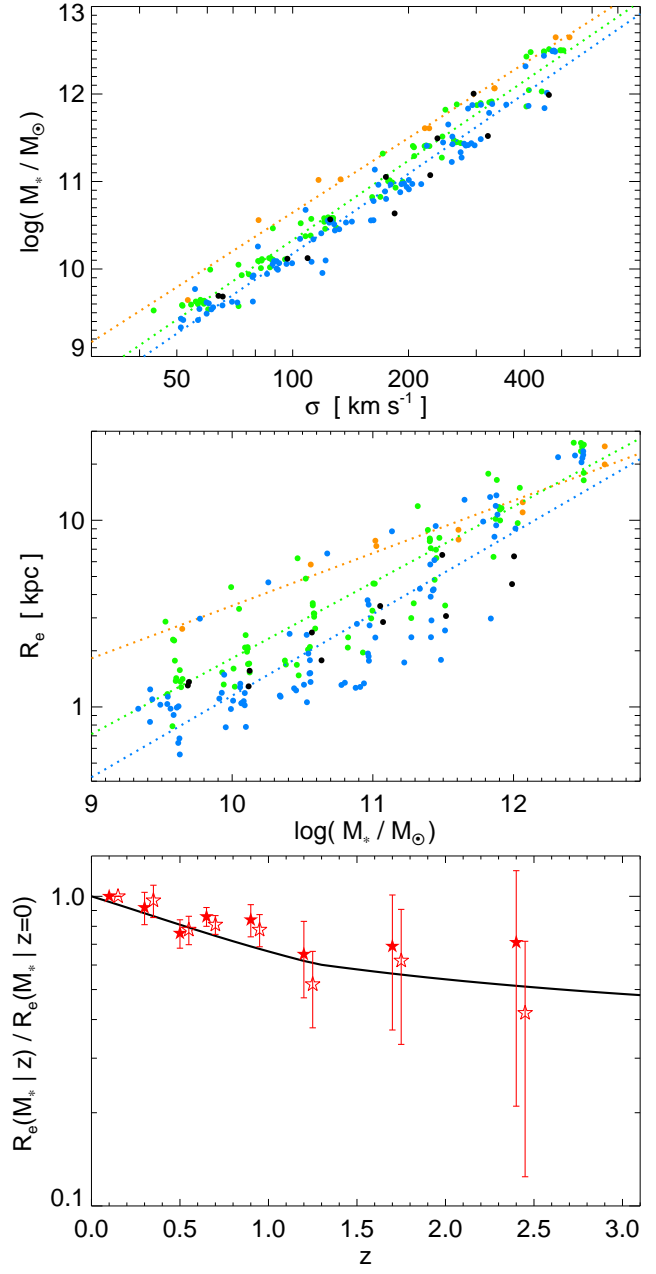


FIG. 19.— *Upper*: Faber-Jackson ($M_* - \sigma$) and $R_e - M_*$ relations in our simulations as a function of gas fraction ($f_{\text{gas}} = 0.2, 0.4, 0.8, 1.0$ in orange, green, blue, and black points, respectively, with the best-fit trend to each as the dotted line of corresponding color). At fixed M_* , higher- f_{gas} systems have smaller R_e and larger σ , as in Figure 14. *Lower*: Given our empirical estimate of the evolution in f_{gas} at fixed $M_* = 10^{11} M_\odot$, and the dependence of $R_e(M_*)$ on f_{gas} (upper panel & Figure 14), solid line plots the expected evolution in $R_e(M_*)$ with redshift. Points compare the observed evolution from Trujillo et al. (2006), for $M_* > 3 \times 10^{10} M_\odot$ (filled) and $M_* > 6 \times 10^{10} M_\odot$ (open). The increasing gas content in high-redshift merger progenitors predicts their size evolution at fixed stellar mass.

Likewise, either directly adopting our fitted trend of M_{BH}/M_* as a function of f_{gas} from Figure 12, or using our estimate of how R_e (and, correspondingly, σ) evolve at fixed M_* with f_{gas} and applying them to the BHFP relation $M_{\text{BH}} \propto M_*^{0.7} \sigma^{1.5} \propto M_*^{1.5} R_e^{-1}$, this predicts that the mean M_{BH}/M_* should increase with redshift. Figures 16 & 17 show the evolution in M_{BH}/M_* expected from this simple derivation. Again, the agreement with the observationally estimated rate

of evolution in M_{BH}/M_* is good.

We do caution that our estimate of the mean evolution in f_{gas} , while consistent with the observational constraints on gas fractions and specific star formation rates at all redshifts with which we compare ($z \lesssim 3$), is only intended as a rough lowest-order approximation to realistic disk evolution. It is of course possible that other disk properties, such as the Tully-Fisher relation, begin to evolve at high redshift (see e.g. Genzel et al. 2006), or that elliptical formation at high redshift might proceed in more chaotic multiple mergers for which our simple approximations are not valid, especially in the most massive systems at very high redshifts $z \sim 6$. However, we have seen in Figure 11 that evolution in properties such as virial velocities, disk structure, and orbital parameters do not drive much additional evolution in M_{BH}/M_* . Furthermore, some reassurance comes from Li et al. (2006), who consider simulations which adopt cosmologically-derived merger histories for the brightest $z \sim 6$ quasars, involving multiple major and minor mergers, and find that the remnant obeys a similar M_{BH}/M_* relation to our idealized high- f_{gas} simulations – i.e. it is consistent with our estimated evolution in M_{BH}/M_* (and R_e/M_*) as a function of redshift. Despite a chaotic, rapid merger history, the remnant properties can approximately be predicted as a function of stellar mass and gas fraction from our simple prescription. The most important (at lowest order) element of our estimate is simply the qualitative statement that the progenitors of high-redshift ellipticals should be characteristically more gas-rich – which given the rapid star-formation timescales estimated for massive disks (Bell & de Jong 2000) and observationally inferred brief, potentially burst-dominated star-formation histories of the most massive ellipticals (e.g., Thomas et al. 2005), is naturally expected in theories of hierarchical growth. In other words, so long as the total stellar mass being violently scattered and total gas supply reaching the spheroid center (i.e. total mass and gas fraction) are similar, the details of the merger history and distinction between binary or multiple mergers should not significantly change the simple gravitational physics which determine the most basic elements of the remnant structure. We therefore suggest that evolution in f_{gas} is indeed the dominant (although not the only) physical agent driving evolution in the $M_{\text{BH}} - M_*$ relation.

9. DISCUSSION

Using a large set of numerical simulations of major galaxy-galaxy mergers, which include the effects of gas dissipation, cooling, star formation, and black hole accretion, we find that a feedback-driven model of BH growth and self-regulation predicts the existence of a BH “fundamental plane” (BHFP), of the form $M_{\text{BH}} \propto \sigma^{3.0} R_e^{0.5}$ or $M_{\text{BH}} \propto M_*^{0.5-0.7} \sigma^{1.5-2.0}$, analogous to the FP of spheroids. Comparing with existing BH mass measurements, the observed systems appear to follow a nearly identical BHFP relation. Specifically, there are significant ($> 99.9\%$ confidence) trends in the residuals of the $M_{\text{BH}} - \sigma$ relation with M_* and R_e at fixed σ , and likewise in the $M_{\text{BH}} - M_*$ relation (with σ or R_e at fixed M_*). While changes in halo circular velocity, merger orbital parameters, progenitor disk redshifts and gas fractions, ISM gas pressurization, and other parameters can drive changes in e.g. σ at fixed M_* , and therefore change in the $M_{\text{BH}} - \sigma$ or $M_{\text{BH}} - M_*$ relations, the BHFP is preserved.

This provides a new paradigm for understanding the traditional relations between BH mass and either bulge velocity dispersion or mass. These correlations (as well as those

with other bulge properties such as effective radius, central potential, dynamical mass, concentration, Sersic index, and bulge binding energy) are all projections of the same fundamental plane relation. Just as the Faber-Jackson relation between e.g. stellar mass or luminosity and velocity dispersion ($M_* - \sigma$) is understood as a projection of the more fundamental relation between M_* , σ , and R_e , so too is the $M_{\text{BH}} - \sigma$ relation ($M_{\text{BH}} \propto \sigma^4$) a projection of the more fundamental relation $M_{\text{BH}} \propto \sigma^3 R_e^{0.5}$. Recognizing this resolves the nature of several apparent outliers in the $M_{\text{BH}} - \sigma$ relation, which simply have unusual σ values for their stellar masses or effective radii, and eliminates the strong correlations between residuals (in both observations and simulations). While the various changes above in merger properties can and do bias the various projections of the BHFP to different values, they simply move remnants *along* the BHFP relation.

Given the empirical tendency towards more compact, smaller- R_e spheroids at fixed stellar mass M_* at high redshift, the BHFP predicts that BHs should be more massive at fixed M_* . Trujillo et al. (2006) compile a number of observations of the sizes of early-type galaxies at fixed stellar mass (for typical $\sim L_*$ galaxies), and find a best-fit trend $R_e \propto (1+z)^{-0.45}$. The observed BHFP predicts that BH mass scales roughly as $\propto M_*^{1.5} R_e^{-1.0}$, which yields the prediction that the typical hosted BH mass at fixed stellar mass (or ratio of M_{BH}/M_*) should increase as $(1+z)^{0.5}$. This agrees well with recent direct estimates of the BH to host stellar mass ratio at high redshift (Peng et al. 2006), as well as indirect estimates of the evolution in the mean M_{BH}/M_* from comparisons of quasar luminosity functions and early-type mass density measurements (Merloni et al. 2004), BH and spheroid mass functions (Hopkins et al. 2006d), and quasar clustering as a function of redshift (Adelberger & Steidel 2005; Wyithe & Loeb 2005; Hopkins et al. 2007e; Fine et al. 2006). Interestingly, if we consider this in greater detail, observations suggest that the evolution in spheroid sizes is relatively weak to $z \sim 0.8$ (McIntosh et al. 2005) and stronger from $z \sim 1-2$. Our BHFP analysis argues that the same should be true for the ratio of BH mass to stellar mass, and indeed Peng et al. (2006) note that there is no significant evolution at lower redshifts $z \lesssim 1$ in their sample, compared to the substantial evolution they observe at $z \sim 1-3$.

We have also developed a physically motivated model for this evolution. Based on the empirical and theoretical expectation that the progenitor disks in typical mergers should be more gas-rich at higher redshifts, we expect mergers to be more dissipational, yielding more concentrated remnants and driving the evolution in M_{BH}/M_* along the BHFP. Indeed, adopting an empirical estimate for the mean f_{gas} as a function of stellar mass and redshift, we predict a trend with redshift in the size-mass relation of our merger remnants which is similar to the observations compiled in Trujillo et al. (2006), and consequently a trend in M_{BH}/M_* like that observed by Peng et al. (2006). Our simulations thus provide critical support to arguments from a semi-analytic context, such as those made by Khochfar & Silk (2006), that the observed evolution in $R_e(M_*)$ can be explained by the increasingly gas-rich, dissipational nature of merger progenitors at high redshifts. It is worth noting that, although it does not rule out such mergers occurring, the trend in $R_e(M_*)$ can be explained entirely by changing gas fractions in gas-rich, dissipational mergers, *without* invoking subsequent “dry” mergers at low redshifts to increase R_e (see also, Krause et al. 2007, in preparation).

We also emphasize that our results are entirely consistent with the previous study of Robertson et al. (2006c). However, in that case, the authors considered only the effects of the (relatively weak) scaling of disk sizes at fixed M_* with redshift, and found that this introduced a weak evolution in the $M_{\text{BH}} - \sigma$ relation. Allowing for f_{gas} to scale systematically with redshift drives the evolution in M_{BH}/M_* which is analyzed herein, and placing both simulations and observations in the context of the FP relation reconciles the apparent disagreement between the predictions of Robertson et al. (2006c) for the $M_{\text{BH}} - \sigma$ relation and observations by e.g. Peng et al. (2006) of the high-redshift $M_{\text{BH}} - M_*$ relation.

There are a number of direct, testable predictions of this fundamental plane model for the correlations between BH and host properties. At both low and high redshifts, systems should lie on the same BHFP. Therefore, measurements of the effective radii or velocity dispersions of the Peng et al. (2006) objects should find that they are more compact (smaller R_e , larger σ) than their $z=0$ counterparts of the same stellar mass, in a manner consistent with the BHFP in Table 1. If it is really the BHFP driving the apparent evolution in M_{BH}/M_* with redshift, i.e. the fact that at fixed M_* , higher-redshift systems are more compact, then this also predicts different evolution for BH mass relative to σ (the $M_{\text{BH}} - \sigma$ relation) than for BH mass relative to M_* . Adopting the Trujillo et al. (2006) estimate for how R_e scales with redshift and the near-IR spheroid fundamental plane of Pahre et al. (1998) to relate σ and R_e at fixed M_* , along with our BHFP in terms of M_* and σ , this predicts a trend of the form $M_{\text{BH}}/\sigma^4 \propto (1+z)^{-0.25}$, i.e. weaker and *inverse* evolution in M_{BH}/σ at fixed stellar mass, quite similar to the predictions made by Robertson et al. (2006c) and consistent with the observations of Shields et al. (2003).

At low redshifts, improved measurements of the host properties of systems with well-measured BHs can significantly improve constraints on the BHFP. As noted in Table 1, the present observations demand a correlation of the form $M_{\text{BH}} \propto \sigma^\alpha M_*^\beta$ over a simple correlation with either σ or M_* at $\gtrsim 3\sigma$ confidence. Already, this puts strong constraints on theoretical models of BH growth and evolution – BH mass does not simply scale with the star formation (stellar mass) or virial velocity of the host galaxy. However, there is still a substantial degeneracy between the slopes α and β (roughly along the axis $\beta \approx 1 - \alpha/4$). For example, the current data do not allow us to significantly distinguish a pure correlation with spheroid binding energy $M_{\text{BH}} \propto (M_* \sigma^2)^{2/3}$ from the marginally favored relation $\propto M_*^{1/2} \sigma^2$ – both suggest that the ability of BHs to self-regulate their growth must be sensitive to the potential well at the center of the galaxy (and therefore to galactic structure), but the difference could reveal variations in the means by which BH feedback couples to the gas on these scales.

Increasing the observed sample sizes and, in particular, extending the observed baselines in mass and σ will substantially improve the lever arm on these correlations. In particular, the addition of stellar mass M_* information to the significant number of objects which have measurements of σ and indirect measurements of M_{BH} from reverberation mapping would enable considerably stronger tests of our proposed BHFP relation. Furthermore, to the extent that the evolution in the M_{BH}/M_* and $R_e(M_*)$ relations is driven by

the relatively gas-rich nature of the merger progenitors, the residuals in e.g. M_{BH}/M_* should also be correlated with other tracers of the amount of dissipation in the spheroid-forming merger. These include quantities such as R_e and σ , of course, in the context we have discussed, but also e.g. the central phase-space density, kinematic properties such as rotation and kinematically decoupled components (see Hernquist & Barnes 1991; Cox et al. 2006b), and potentially the presence of central cusps in the stellar light profiles of the remnants (Mihos & Hernquist 1994a). We do note the caveat from § 7, however, that care should still be taken to consider only bulge properties and remove e.g. rotationally supported contributions to the velocity dispersion.

Given the robust nature of the BHFP, we might also ask if there are processes which we might expect to drive systems away from the BHFP. For example, what are the effects of subsequent gas-poor (spheroid-spheroid or “dry”) mergers on the BHFP? Such mergers, by definition, conserve total stellar mass and BH mass (simply adding the M_* and M_{BH} of the two merged systems). However, simple energetic arguments imply that σ is not dramatically changed (e.g., Hernquist et al. 1993; Nipoti et al. 2003; Boylan-Kolchin et al. 2006). If we assume σ is unchanged in a “dry” merger, then the BHFP relations in Table 1 imply a $\sim 0.08 - 0.12$ dex offset (in the sense of M_{BH} being too large) from a major (equal-mass) dry merger (the offset being $\sim 0.03 - 0.05$ dex for a more probable 1:3 mass-ratio merger). This is also supported by a small subset of full numerical re-merger simulations from Robertson et al. (2006b). Although this implies that the BHFP will not survive a large number ($\gtrsim 3$) of successive dry mergers, the observationally estimated rate of $\sim 0.5 - 1$ major dry mergers for a typical massive elliptical (Bell et al. 2006; van Dokkum 2005) implies that the realistic resulting deviations from the BHFP are small (smaller than the internal scatter in the relation itself). This may be important, however, for explaining how the compact, high-redshift spheroids observed and predicted herein increase in size to lie on the local $R_e - M_*$ relations (since each major dry merger will approximately double R_e), a possibility that will be investigated in detail in future work.

Therefore, as appears to be borne out by the local observations we consider, the BHFP appears to be a robust correlation, which provides an improved context in which to understand the nature and evolution of the numerous observed correlations between BH and host spheroid properties. In particular, the results described here provide new, important constraints for models of BH growth, feedback and self-regulation, and support the proposal developed by Hopkins et al. (2006a) that major mergers between gas-rich galaxies represent the principle mechanism for triggering intense starbursts (e.g., Barnes & Hernquist 1991; Mihos & Hernquist 1994b, 1996) that evolve into quasars (e.g., Sanders et al. 1988) and which eventually leave remnants satisfying the same structural correlations observed for elliptical galaxies (e.g., Robertson et al. 2006b).

We thank Chien Peng for illuminating discussion and comments. This work was supported in part by NSF grant AST 03-07690, and NASA ATP grants NAG5-12140, NAG5-13292, and NAG5-13381.

REFERENCES

Adelberger, K. L., & Steidel, C. C. 2005, ApJ, 627, L1

Aller, M. C., & Richstone, D. O. 2007, ApJ, accepted, arXiv:0705.1165v1 [astro-ph], 705

Barnes, J. E., & Hernquist, L. E. 1991, *ApJ*, 370, L65

Batcheldor, D., Marconi, A., Merritt, D., & Axon, D. J. 2006, *ApJ*, in press [astro-ph/0610264]

Bauer, A. E., Drory, N., Hill, G. J., & Feulner, G. 2005, *ApJ*, 621, L89

Bell, E. F., & de Jong, R. S. 2000, *MNRAS*, 312, 497

—. 2001, *ApJ*, 550, 212

Bell, E. F., McIntosh, D. H., Katz, N., & Weinberg, M. D. 2003, *ApJS*, 149, 289

Bell, E. F., Naab, T., McIntosh, D. H., Somerville, R. S., Caldwell, J. A. R., Barden, M., Wolf, C., Rix, H.-W., Beckwith, S. V., Borch, A., Häussler, B., Heymans, C., Jahnke, K., Jogee, S., Koposov, S., Meisenheimer, K., Peng, C. Y., Sanchez, S. F., & Wisotzki, L. 2006, *ApJ*, 640, 241

Bernardi, M., Sheth, R. K., Tundo, E., & Hyde, J. B. 2006, *ApJ*, in press [astro-ph/0609300]

Bernardi, M., et al. 2003a, *ApJ*, 125, 1849

—. 2003b, *AJ*, 125, 1866

Boylan-Kolchin, M., Ma, C.-P., & Quataert, E. 2006, *MNRAS*, 369, 1081

Bullock, J. S., Kolatt, T. S., Sigad, Y., Somerville, R. S., Kravtsov, A. V., Klypin, A. A., Primack, J. R., & Dekel, A. 2001, *MNRAS*, 321, 559

Burkert, A., & Silk, J. 2001, *ApJ*, 554, L151

Busha, M. T., Evrard, A. E., Adams, F. C., & Wechsler, R. H. 2005, *MNRAS*, 363, L11

Cattaneo, A., Combes, F., Colombi, S., Bertin, E., & Melchior, A.-L. 2005, *MNRAS*, 359, 1237

Cole, S., Norberg, P., Baugh, C. M., Frenk, C. S., Bland-Hawthorn, J., Bridges, T., Cannon, R., Colless, M., Collins, C., Couch, W., Cross, N., Dalton, G., De Propris, R., Driver, S. P., Efstathiou, G., Ellis, R. S., Glazebrook, K., Jackson, C., Lahav, O., Lewis, I., Lumsden, S., Maddox, S., Madgwick, D., Peacock, J. A., Peterson, B. A., Sutherland, W., & Taylor, K. 2001, *MNRAS*, 326, 255

Conroy, C., Prada, F., Newman, J. A., Croton, D., Coil, A. L., Conselice, C. J., Cooper, M. C., Davis, M., Faber, S. M., Gerke, B. F., Guhathakurta, P., Klypin, A., Koo, D. C., & Yan, R. 2007, *ApJ*, 654, 153

Conselice, C. J., Bundy, K., Ellis, R. S., Brichmann, J., Vogt, N. P., & Phillips, A. C. 2005, *ApJ*, 628, 160

Cowie, L. L., Songaila, A., Hu, E. M., & Cohen, J. G. 1996, *AJ*, 112, 839

Cox, T. J., Di Matteo, T., Hernquist, L., Hopkins, P. F., Robertson, B., & Springel, V. 2006a, *ApJ*, 643, 692

Cox, T. J., Dutta, S. N., Di Matteo, T., Hernquist, L., Hopkins, P. F., Robertson, B., & Springel, V. 2006b, *ApJ*, accepted [astro-ph/0607446]

Croton, D. J. 2006, *MNRAS*, 369, 1808

Davé, R., Hernquist, L., Katz, N., & Weinberg, D. H. 1999, *ApJ*, 511, 521

de Francesco, G., Capetti, A., & Marconi, A. 2006, *A&A*, 460, 439

Di Matteo, T., Colberg, J., Springel, V., Hernquist, L., & Sijacki, D. 2007, *ApJ*, submitted, arXiv:0705.2269v1 [astro-ph]

Di Matteo, T., Springel, V., & Hernquist, L. 2005, *Nature*, 433, 604

Djorgovski, S., & Davis, M. 1987, *ApJ*, 313, 59

Dressler, A., Lynden-Bell, D., Burstein, D., Davies, R. L., Faber, S. M., Terlevich, R., & Wegner, G. 1987, *ApJ*, 313, 42

Erb, D. K., Steidel, C. C., Shapley, A. E., Pettini, M., Reddy, N. A., & Adelberger, K. L. 2006, *ApJ*, 646, 107

Faber, S. M., & Jackson, R. E. 1976, *ApJ*, 204, 668

Ferrarese, L., & Merritt, D. 2000, *ApJ*, 539, L9

Feulner, G., Gabasch, A., Salvato, M., Drory, N., Hopp, U., & Bender, R. 2005, *ApJ*, 633, L9

Fine, S., Croom, S. M., Miller, L., Babic, A., Moore, D., Brewer, B., Sharp, R. G., Boyle, B. J., Shanks, T., Smith, R. J., Outram, P. J., & Loaring, N. S. 2006, *MNRAS*, 373, 613

Flores, H., Hammer, F., Puech, M., Amram, P., & Balkowski, C. 2006, *A&A*, 455, 107

Gebhardt, K., et al. 2000, *ApJ*, 539, L13

Genzel, R., Tacconi, L. J., Eisenhauer, F., Förster Schreiber, N. M., Cimatti, A., Daddi, E., Bouché, N., Davies, R., Lehnert, M. D., Lutz, D., Nesvadba, N., Verma, A., Abuter, R., Shapiro, K., Sternberg, A., Renzini, A., Kong, X., Arimoto, N., & Mignoli, M. 2006, *Nature*, 442, 786

Gerhard, O., Kronawitter, A., Saglia, R. P., & Bender, R. 2001, *AJ*, 121, 1936

Graham, A. W., & Driver, S. P. 2006, *ApJ*, in press [astro-ph/0607378]

Graham, A. W., Erwin, P., Caon, N., & Trujillo, I. 2001, *ApJ*, 563, L11

Granato, G. L., De Zotti, G., Silva, L., Bressan, A., & Danese, L. 2004, *ApJ*, 600, 580

Häring, N., & Rix, H.-W. 2004, *ApJ*, 604, L89

Hernquist, L. 1990, *ApJ*, 356, 359

—. 1993, *ApJ*, 404, 717

Hernquist, L., & Barnes, J. E. 1991, *Nature*, 354, 210

Hernquist, L., Spergel, D. N., & Heyl, J. S. 1993, *ApJ*, 416, 415

Heymans, C., Bell, E. F., Rix, H.-W., Barden, M., Borch, A., Caldwell, J. A. R., McIntosh, D. H., Meisenheimer, K., Peng, C. Y., Wolf, C., Beckwith, S. V. W., Häussler, B., Jahnke, K., Jogee, S., Sánchez, S. F., Somerville, R., & Wisotzki, L. 2006, *MNRAS*, 371, L60

Hopkins, P. F., Bundy, K., Hernquist, L., & Ellis, R. S. 2007a, *ApJ*, 659, 976

Hopkins, P. F., Cox, T. J., Keres, D., & Hernquist, L. 2007b, *ApJ*, submitted, arXiv:0706.1246v1 [astro-ph], 706

Hopkins, P. F., & Hernquist, L. 2006, *ApJS*, 166, 1

Hopkins, P. F., Hernquist, L., Cox, T. J., Di Matteo, T., Robertson, B., & Springel, V. 2006a, *ApJS*, 163, 1

Hopkins, P. F., Hernquist, L., Cox, T. J., & Keres, D. 2007c, *ApJ*, submitted, arXiv:0706.1243v1 [astro-ph], 706

Hopkins, P. F., Hernquist, L., Cox, T. J., Robertson, B., Di Matteo, T., & Springel, V. 2006b, *ApJ*, 639, 700

Hopkins, P. F., Hernquist, L., Cox, T. J., Robertson, B., & Krause, E. 2007d, *ApJ*, submitted arXiv:0704.4005v1 [astro-ph] [Paper I]

Hopkins, P. F., Hernquist, L., Cox, T. J., Robertson, B., & Springel, V. 2006c, *ApJS*, 163, 50

Hopkins, P. F., Hernquist, L., Martini, P., Cox, T. J., Robertson, B., Di Matteo, T., & Springel, V. 2005, *ApJ*, 625, L71

Hopkins, P. F., Lidz, A., Hernquist, L., Coil, A. L., Myers, A. D., Cox, T. J., & Spergel, D. N. 2007e, *ApJ*, 662, 110

Hopkins, P. F., Richards, G. T., & Hernquist, L. 2007f, *ApJ*, 654, 731

Hopkins, P. F., Robertson, B., Krause, E., Hernquist, L., & Cox, T. J. 2006d, *ApJ*, 652, 107

Hopkins, P. F., Somerville, R. S., Hernquist, L., Cox, T. J., Robertson, B., & Li, Y. 2006e, *ApJ*, 652, 864

Jones, D. H., Peterson, B. A., Colless, M., & Saunders, W. 2006, *MNRAS*, 369, 25

Kannappan, S. J. 2004, *ApJ*, 611, L89

Katz, N., Weinberg, D. H., & Hernquist, L. 1996, *ApJS*, 105, 19

Kawakatu, N., Anabuki, N., Nagao, T., Umemura, M., Nakagawa, T., & Mori, M. 2006, *New Astronomy Review*, 50, 769

Kennicutt, Jr., R. C. 1998, *ApJ*, 498, 541

Khochfar, S., & Silk, J. 2006, *ApJ*, 648, L21

Kollmeier, J. A., Omken, C. A., Kochanek, C. S., Gould, A., Weinberg, D. H., Dietrich, M., Cool, R., Dey, A., Eisenstein, D. J., Jannuzzi, B. T., Le Floc'h, E., & Stern, D. 2006, *ApJ*, 648, 128

Kormendy, J. 1977, *ApJ*, 218, 333

Kormendy, J., Fisher, D. B., Cornell, M. E., & Bender, R. 2007, *ApJ*, submitted

Kormendy, J., & Richstone, D. 1995, *ARA&A*, 33, 581

Kronawitter, A., Saglia, R. P., Gerhard, O., & Bender, R. 2000, *A&AS*, 144, 53

Lauer, T. R., et al. 2005, *AJ*, 129, 2138

—. 2006a, *ApJ*, in press [astro-ph/0609762]

—. 2006b, *ApJ*, in press [astro-ph/0606739]

Li, Y., Hernquist, L., Robertson, B., Cox, T. J., Hopkins, P. F., Springel, V., Gao, L., Di Matteo, T., Zentner, A. R., Jenkins, A., & Yoshida, N. 2006, *ApJ*, in press [astro-ph/0608190]

Lidz, A., Hopkins, P. F., Cox, T. J., Hernquist, L., & Robertson, B. 2006, *ApJ*, 641, 41

Lin, Y.-T., & Mohr, J. J. 2004, *ApJ*, 617, 879

Magorrian, J., et al. 1998, *AJ*, 115, 2285

Maraschi, L. 2004, *Ap&SS*, 294, 101

Marconi, A., & Hunt, L. K. 2003, *ApJ*, 589, L21

Marconi, A., Risaliti, G., Gilli, R., Hunt, L. K., Maiolino, R., & Salvati, M. 2004, *MNRAS*, 351, 169

Martini, P. 2004, in *Coevolution of Black Holes and Galaxies*, ed. L. C. Ho, 169–+

McDermid, R. M., et al. 2006, *MNRAS*, 1312

McGaugh, S. S. 2005, *ApJ*, 632, 859

McIntosh, D. H., Bell, E. F., Rix, H.-W., Wolf, C., Heymans, C., Peng, C. Y., Somerville, R. S., Barden, M., Beckwith, S. V. W., Borch, A., Caldwell, J. A. R., Häussler, B., Jahnke, K., Jogee, S., Meisenheimer, K., Sánchez, S. F., & Wisotzki, L. 2005, *ApJ*, 632, 191

Merloni, A., Heinz, S., & Di Matteo, T. 2005, *Ap&SS*, 300, 45

Merloni, A., Rudnick, G., & Di Matteo, T. 2004, *MNRAS*, 354, L37

Merritt, D., & Ferrarese, L. 2001, *ApJ*, 547, 140

Mihos, J. C., & Hernquist, L. 1994a, *ApJ*, 437, L47

—. 1994b, *ApJ*, 431, L9

—. 1996, *ApJ*, 464, 641

Mo, H. J., & White, S. D. M. 1996, *MNRAS*, 282, 347

Monaco, P., & Fontanot, F. 2005, *MNRAS*, 359, 283

Murray, N., Quataert, E., & Thompson, T. A. 2005, *ApJ*, 618, 569

Myers, A. D., Brunner, R. J., Nichol, R. C., Richards, G. T., Schneider, D. P., & Bahcall, N. A. 2006, *ApJ*, in press [astro-ph/0612190]

Navarro, J. F., Frenk, C. S., & White, S. D. M. 1996, *ApJ*, 462, 563

Nipoti, C., Londrillo, P., & Ciotti, L. 2003, *MNRAS*, 342, 501

Noeske, K. G., Faber, S. M., Weiner, B. J., Koo, D. C., Primack, J. R., Dekel, A., Papovich, C., Conselice, C. J., Le Floc'h, E., Rieke, G. H., Coil, A. L., Lotz, J. M., Somerville, R. S., & Bundy, K. 2007, *ApJ*, in press [astro-ph/0703056]

Novak, G. S., Faber, S. M., & Dekel, A. 2006, *ApJ*, 637, 96

O'Shea, B. W., Nagamine, K., Springel, V., Hernquist, L., & Norman, M. L. 2005, *ApJS*, 160, 1

Pahre, M. A., Djorgovski, S. G., & de Carvalho, R. R. 1998, *AJ*, 116, 1591

Papovich, C., Moustakas, L. A., Dickinson, M., Le Floc'h, E., Rieke, G. H., Daddi, E., Alexander, D. M., Bauer, F., Brandt, W. N., Dahmen, T., Egami, E., Eisenhardt, P., Elbaz, D., Ferguson, H. C., Giavalisco, M., Lucas, R. A., Mobasher, B., Pérez-González, P. G., Stutz, A., Rieke, M. J., & Yan, H. 2006, *ApJ*, 640, 92

Peng, C. Y., Impey, C. D., Rix, H.-W., Kochanek, C. S., Keeton, C. R., Falco, E. E., Lehár, J., & McLeod, B. A. 2006, *ApJ*, 649, 616

Porciani, C., & Norberg, P. 2006, *MNRAS*, 371, 1824

Robertson, B., Bullock, J. S., Cox, T. J., Di Matteo, T., Hernquist, L., Springel, V., & Yoshida, N. 2006a, *ApJ*, 645, 986

Robertson, B., Cox, T. J., Hernquist, L., Franx, M., Hopkins, P. F., Martini, P., & Springel, V. 2006b, *ApJ*, 641, 21

Robertson, B., Hernquist, L., Cox, T. J., Di Matteo, T., Hopkins, P. F., Martini, P., & Springel, V. 2006c, *ApJ*, 641, 90

Sanders, D. B., Soifer, B. T., Elias, J. H., Madore, B. F., Matthews, K., Neugebauer, G., & Scoville, N. Z. 1988, *ApJ*, 325, 74

Shapley, A. E., Coil, A. L., Ma, C.-P., & Bundy, K. 2005, *ApJ*, 635, 1006

Shen, S., Mo, H. J., White, S. D. M., Blanton, M. R., Kauffmann, G., Voges, W., Brinkmann, J., & Csabai, I. 2003, *MNRAS*, 343, 978

Sheth, R. K., Bernardi, M., Schechter, P. L., Burles, S., Eisenstein, D. J., Finkbeiner, D. P., Frieman, J., Lupton, R. H., Schlegel, D. J., Subbarao, M., Shimasaku, K., Bahcall, N. A., Brinkmann, J., & Ivezić, Ž. 2003, *ApJ*, 594, 225

Sheth, R. K., Mo, H. J., & Tormen, G. 2001, *MNRAS*, 323, 1

Shields, G. A., Gebhardt, K., Salviander, S., Wills, B. J., Xie, B., Brotherton, M. S., Yuan, J., & Dietrich, M. 2003, *ApJ*, 583, 124

Shields, G. A., Menezes, K. L., Massart, C. A., & Vanden Bout, P. 2006, *ApJ*, 641, 683

Sijacki, D., Springel, V., Di Matteo, T., & Hernquist, L. 2007, *MNRAS*, submitted, arXiv:0705.2238v1 [astro-ph]

Silk, J., & Rees, M. J. 1998, *A&A*, 331, L1

Soltan, A. 1982, *MNRAS*, 200, 115

Springel, V. 2005, *MNRAS*, 364, 1105

Springel, V., Di Matteo, T., & Hernquist, L. 2005, *MNRAS*, 361, 776

Springel, V., & Hernquist, L. 2002, *MNRAS*, 333, 649

—. 2003, *MNRAS*, 339, 289

—. 2005, *ApJ*, 622, L9

Tavecchio, F., Maraschi, L., Sambruna, R. M., Urry, C. M., Cheung, C. C., Gambill, J. K., & Scarpa, R. 2004, *ApJ*, 614, 64

Thomas, D., Maraston, C., Bender, R., & Mendes de Oliveira, C. 2005, *ApJ*, 621, 673

Tremaine, S., et al. 2002, *ApJ*, 574, 740

Trujillo, I., Förster Schreiber, N. M., Rudnick, G., Barden, M., Franx, M., Rix, H.-W., Caldwell, J. A. R., McIntosh, D. H., Toft, S., Häussler, B., Zirm, A., van Dokkum, P. G., Labb  , I., Moorwood, A., R  tgering, H., van der Wel, A., van der Werf, P., & van Starkenburg, L. 2006, *ApJ*, 650, 18

Tundo, E., Bernardi, M., Hyde, J. B., Sheth, R. K., & Pizzella, A. 2006, *ApJ*, in press [astro-ph/0609297]

van Dokkum, P. G. 2005, *AJ*, 130, 2647

Vitvitska, M., Klypin, A. A., Kravtsov, A. V., Wechsler, R. H., Primack, J. R., & Bullock, J. S. 2002, *ApJ*, 581, 799

Walter, F., Carilli, C., Bertoldi, F., Menten, K., Cox, P., Lo, K. Y., Fan, X., & Strauss, M. A. 2004, *ApJ*, 615, L17

Woo, J.-H., Treu, T., Malkan, M. A., & Blandford, R. D. 2006, *ApJ*, 645, 900

Wyithe, J. S. B. 2006, *MNRAS*, 365, 1082

Wyithe, J. S. B., & Loeb, A. 2005, *ApJ*, 621, 95

Yu, Q., & Lu, Y. 2004, *ApJ*, 602, 603

Yu, Q., & Tremaine, S. 2002, *MNRAS*, 335, 965

Zheng, Z., Coil, A. L., & Zehavi, I. 2007, *ApJ*, in press [astro-ph/0703457]